[American Journal of Science, Vol. 301, April/May, 2001, P. 385–431]

A FLUVIAL RECORD OF LONG-TERM STEADY-STATE UPLIFT AND EROSION ACROSS THE CASCADIA FOREARC HIGH, WESTERN WASHINGTON STATE

FRANK J. PAZZAGLIA* and MARK T. BRANDON**

ABSTRACT. Six late Quaternary river terraces, preserved along the Clearwater River in northwestern Washington State, provide a ~140 ka record of long-term incision and uplift across the western side of the Cascadia forearc high. Terrace ages are constrained by weathering rind and radiocarbon dating and by correlation to dated coastal glacio-fluvial deposits and the global eustatic curve. The terraces overlie flat bedrock surfaces, called straths, which represent uplifted segments of the river channel. Bedrock incision is measured by the height of a strath relative to the adjacent modern river channel. The straths along the Clearwater show an upstream increase in bedrock incision, ranging from ~0 at the coast to a maximum of 110 m in the headwaters. The incision at any point along the profile increases systematically with strath age. The calculated incision rates range from <0.1 m/ky at the coast, to ~0.9 m/ky in the central massif of the Olympic Mountains. These rates are in close agreement with published long-term erosion rates estimated from fission-track cooling ages. The coincidence between bedrock incision rates and erosion rates suggests that over the long term (>~10 ky) the Clearwater River valley has maintained a steady-state profile defined by a long-term balance in the rates of incision and rock uplift. Upstream divergence of terraces is best explained by an increase in the rate of rock uplift from the coast toward the central part of the range. These results are consistent with other evidence indicating a long-term steady-state balance between the accretionary influx and the erosional outflux for this part of the Cascadia subduction wedge since ~14 Ma.

These results help show how terrace deposits form in tectonically active landscapes. The dominantly fluvial Clearwater drainage was forming straths while alpine glaciers were advancing in adjacent drainages. In turn, the straths were buried during the transition to interglacial times because of increased sediment supply due to local deglaciation and because of eustatic highstands that forced aggradation in the lower reach of the drainage and across the continental shelf as well. The fluvial system shows strong forcing by the glacial climate cycle. Even so, the river appears to have returned to the same valley profile during each cycle of strath cutting. Thus, bedrock incision is clearly unsteady at time scales shorter than the glacial climate cycle (~100 Ky) but appears to be relatively steady when averaged over longer time scales.

A simple kinematic model is used to examine how uplift of the Cl . Our analysis indicates that the accretionary flux into the wedge occurs mainly by frontal accretion and not by underplating. If accretion occurred entirely at the front of the wedge, the present west coast should be moving to the northeast at ~3 m/ky, relative to a fixed Puget Sound. This prediction is in good agreement with offset of a ~122 ka sea cliff preserved at the southwest side of the Clearwater valley profile. In this case, the long-term margin-perpendicular shortening would account for 20 to 35 percent of the geodetically-measured northeast-southwest shortening across the Olympic Mountains.

INTRODUCTION

Mountains come into being where rock uplift outpaces erosion. Growth of topography generally coincides with increases in erosion rate, as long as the topography continues to receive significant precipitation. Thus, with time, we might expect that erosion will become fast enough to balance rock uplift, resulting in a steady-state

* Department of Earth and Environmental Sciences, Lehigh University, 31 Williams, Bethlehem, Pennsylvania 18015

** Department of Geology and Geophysics, Yale University, P.O. Box 208109, New Haven, Connecticut 06520-8109

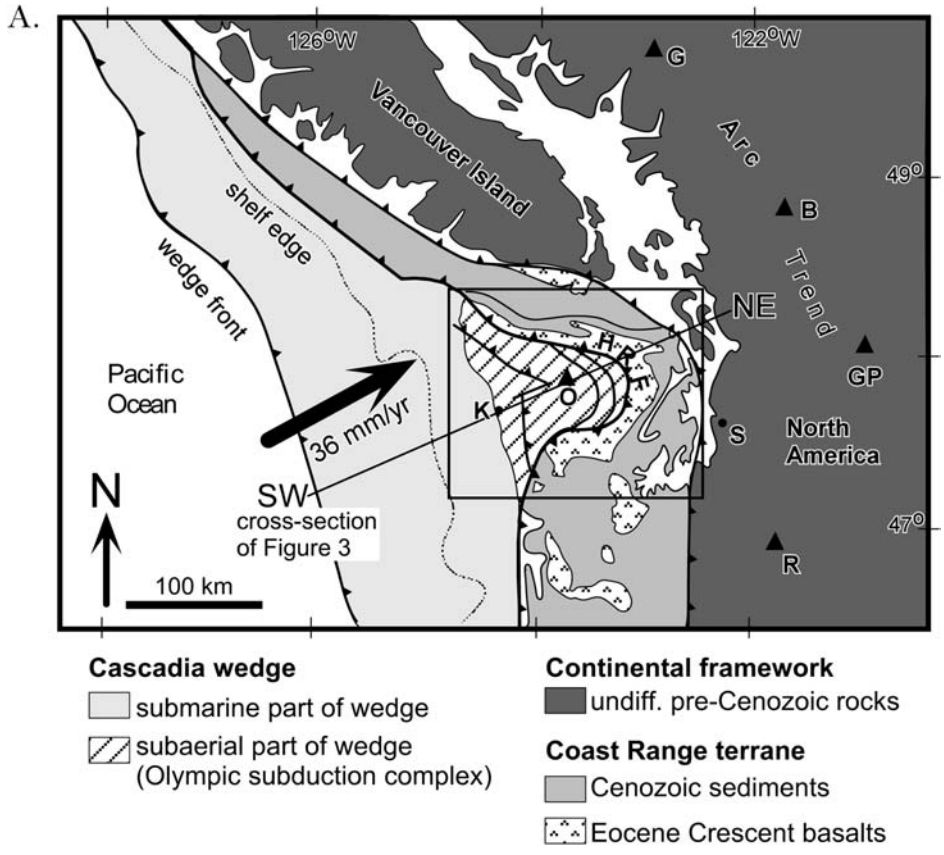

Fig. 1(A) Simplified geologic map of the Cascadia convergent margin, modified from Brandon, Roden-Tice, Garver (1998). HRF = Hurricane Ridge Fault, K = Kalaloch, S = Seattle, O = Mt. Olympus, G = Mt. Garibaldi, B = Mt. Baker, GP = Glacier Peak, R = Mt. Rainier. Beneath the Olympics, the convergence velocity of the Juan de Fuca plate relative to North America is 36 mm/yr at 54°, which is nearly orthogonal to the modern subduction zone (option 2 for Juan de Fuca/Pacific in DeMets and others, 1990, and "NA-PA Combined" in DeMets and Dixon, 1999).

balance between the accretionary flux into the orogen (that is,"tectonic uplift") and the erosional flux out of the orogen (Brandon, Roden-Tice, and Garver, 1998; Hovius, 2000). The amount of time needed to reach steady state depends on the accretionary flux, the erosional processes, and the final steady-state size of the orogen. Some orogens appear to reach a flux steady state within several million years (for example, Southern Alps of New Zealand, Taiwan Alps), whereas others will probably never reach this steady state because of the development of an orographic rain shadow (for example, Himalayan-Tibet, Andes) or because the orogen remains entirely below sealevel (for example, Barbados subduction wedge).

In this paper, we use fluvial geomorphology to test the hypothesis that the Olympic Mountains sector (fig. 1) of the Cascadia convergent margin is presently in a flux steady state (Brandon, Roden-Tice, and Garver, 1998). The seismic hazard potential of this margin has received considerable attention in recent years. Of particular interest is detailed evidence of large subduction-related earthquakes (Savage, Lisowski, and Prescott, 1981, 1991; Atwater, 1987, 1996; Dragert, 1987; Rogers, 1988; Hyndman and Wang, 1993; Darienzo and Peterson, 1990; Bucknam, Hemphill-

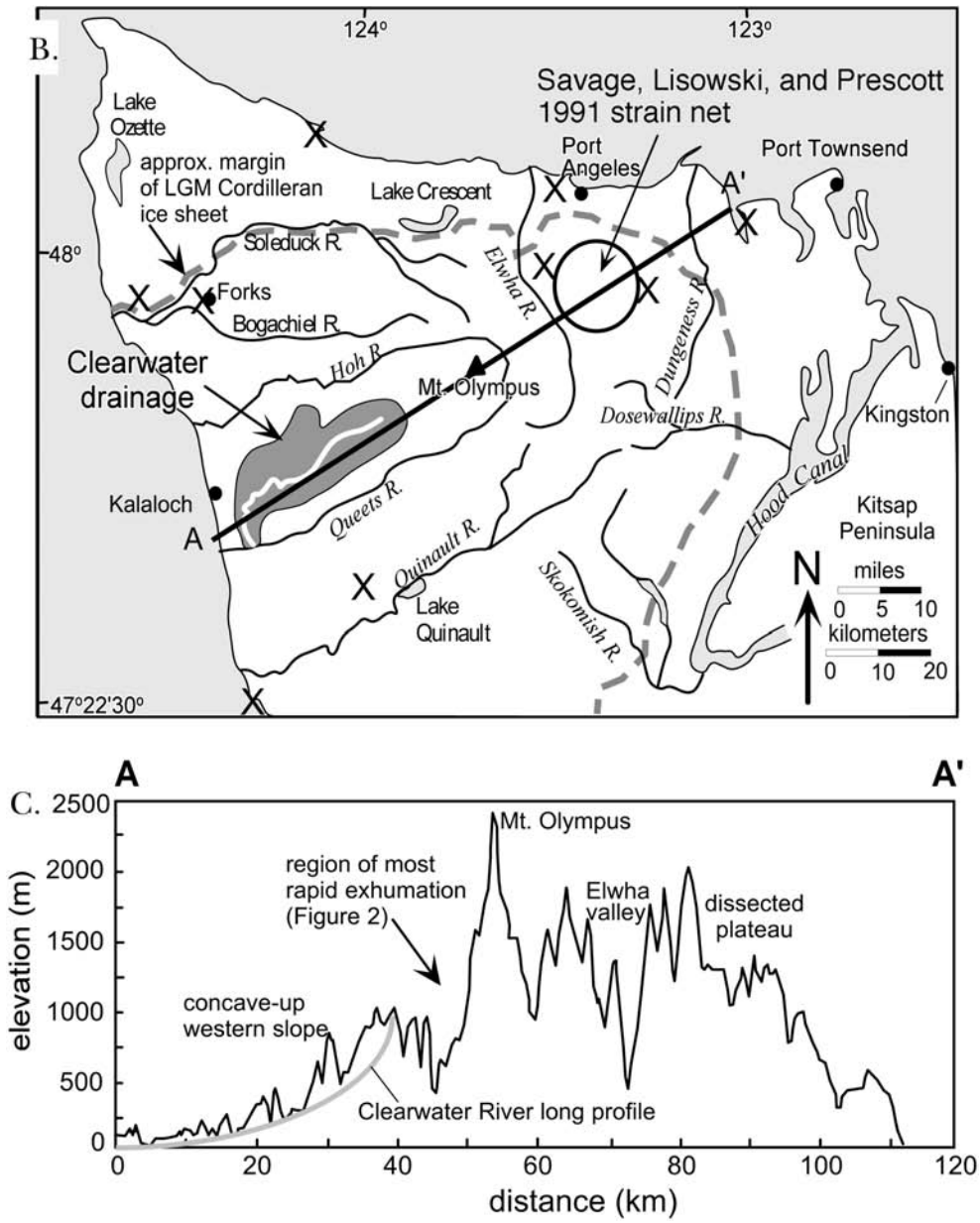

Fig. 1 (continued) (B) Major drainages of the Olympic Peninsula. The gray dashed line marks the southern boundary of the last glacial maxima (LGM) of the Cordilleran ice sheet. X = benchmarks for GPS data shown in figure 21. (C) Topographic section across the Olympic Peninsula, parallel to the modern convergence direction (A-A′ in B).

Haley, and Leopold, 1992; Dragert and others, 1994; Mitchell and others, 1994). Fundamental to these studies is the distinction between short-term ($< \sim$1 ky) cyclic elastic deformation adjacent to the seismogenic subduction thrust and long-term ($> \sim$10 ky) permanent deformation associated with growth and deformation of the

overlying Cascadia subduction wedge (fig. 2). Holocene deposits preserved in locally subsiding estuaries along the west coast provide good evidence of the cyclic deformation related to large prehistoric earthquakes (Atwater, 1987, 1996). It remains difficult to separate elastic deformation, which is created and then recovered during each earthquake cycle, from the permanent deformation associated with fault slip and within-wedge ductile flow.

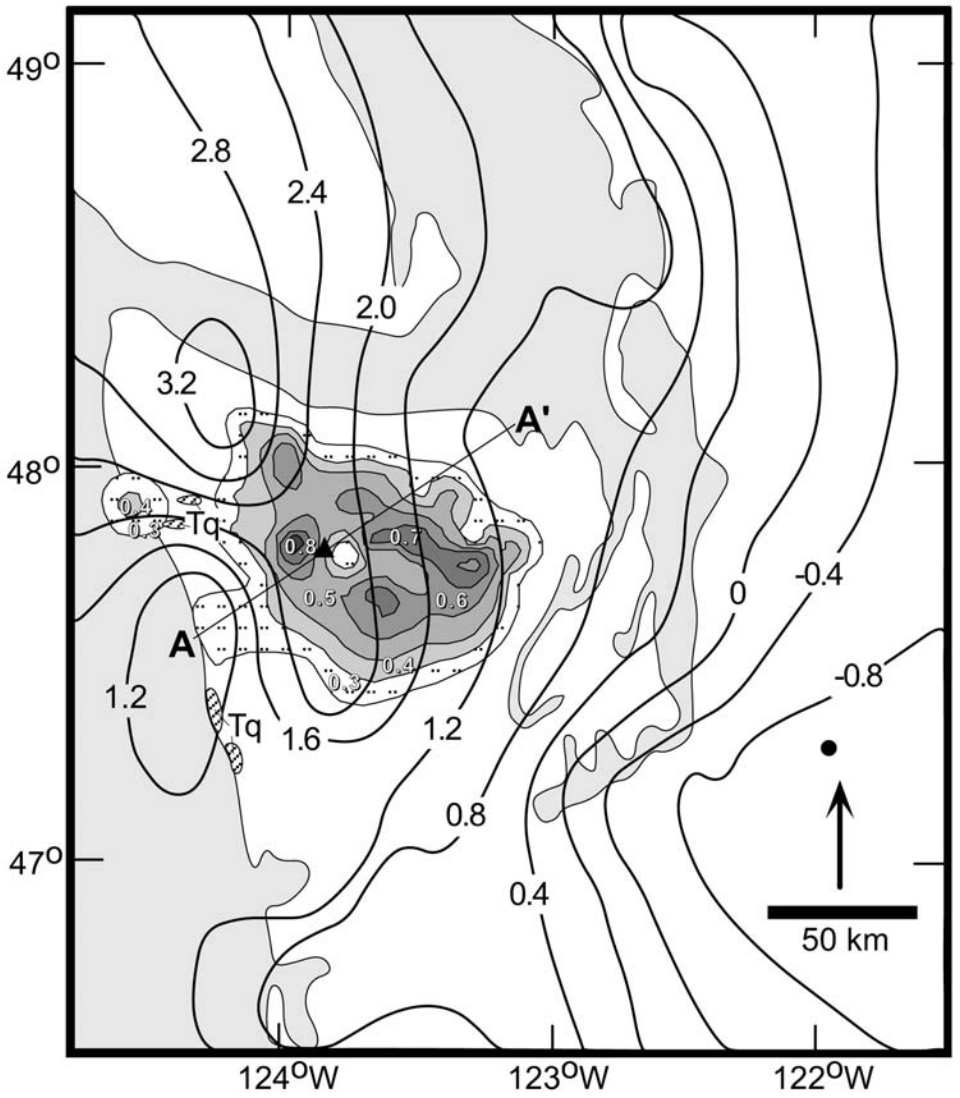

Fig. 2. Contour map showing short-term uplift rates (solid contour lines) as determined by geodetic measurements (Savage, Lisowiski, and Prescott, 1991; Dragert and others, 1994) and long-term erosion rates (shaded contour intervals) as determined by fission-track thermochronology (Brandon, Roden-Tice, and Garver, 1998, and M. Brandon and M. Roden-Tice, unpublished apatite fission-track ages). Rates are in mm/yr. Areas labeled Tq (diagonal-ruled pattern) along the west coast mark exposures of lower Pliocene shallow marine sediments of the Quinault Formation. The preservation of the Quinault and other adjacent near shore units indicates slow long-term uplift and erosion along the west coast.

Pre-Holocene stratigraphy provides the only record of sufficient duration to average out the elastic deformation related to the earthquake cycle. This realization has driven an increased study of the deformation of Quaternary deposits and landforms, but such features are generally restricted to coastal and other lowland areas and the continental shelf as well (Rau, 1973, 1975, 1979; Adams, 1984; West and McCrumb, 1988; Kelsey, 1990; Bockheim, Kelsey, and Marshall, 1992; Kelsey and Bockheim, 1994; Thackray and Pazzaglia, 1994; McCrory, 1996, 1997; McNeill and others, 1997, 2000; Thackray, 1998). In contrast, less is known about the long-term uplift and deformation of the coastal mountains of western Oregon, western Washington, and Vancouver Island because the topography of this highland preserves little stratigraphic evidence of its uplift history. The Oregon-Washington Coast Range and the Insular Mountains of Vancouver Island mark the forearc high of the modern Cascadia wedge. This mountain range parallels the modern subduction zone for ~900 km from southern Oregon to northern Vancouver Island. The development and maintenance of this topographic high provides clear evidence that it is an actively deforming part of the Cascadia plate boundary. Personius (1995), Yeats (1996), and McNeill and others (2000) document the active emergence of the Oregon Coast Range over the last 10 to 15 my. The Washington Coast Range shows a similar emergence history, which is best documented in the Olympic Mountains (fig. 1B, C) (Brandon, Roden-Tice, and Garver, 1998).

The Olympic Mountains occupy a 5800 km^2 area within the Olympic Peninsula. The central part of the range has an average elevation of ~1200 m and reaches a maximum of 2417 m at Mount Olympus (fig. 1C). The Olympics first emerged above sealevel at ~18 Ma (Brandon and Vance, 1992) and then seem to quickly reach a flux steady state (Brandon, Roden-Tice, and Garver, 1998). Fission-track cooling ages indicate that the fastest erosion rates (~0.8 m/ky) are localized in the highest part of the range (fig. 2). Rocks exposed there were deposited and accreted in the Cascadia trench during the late Oligocene and early Miocene and then exhumed from a depth of ~12 to 14 km over the last 16 my. Present-day rugged relief and high-standing topography are consistent with ongoing tectonic uplift.

Geodetic and tide gauge data (Reilinger and Adams, 1982; Holdahl, Faucher, and Dragert, 1989; Savage, Lisowski, and Prescott, 1991; Mitchell and others, 1994) indicate that short-term uplift is very fast in the Olympic Peninsula, ranging from 1.2 to 3.2 m/ky, with the highest rates along the west side of the peninsula (fig. 2). These large rates probably include a significant component of earthquake-cycle elastic deformation, given that the Cascadia subduction thrust is presently locked. This conclusion is supported by geologic evidence that indicates little to no long-term uplift along the east and west coasts of the peninsula over the last 10 my. For instance, exposures of upper Miocene to lower Pliocene shallow marine deposits locally crop out near modern sealevel (for example, Montesano and Quinault formations; see Tq in fig. 2) (Rau, 1970; Tabor and Cady, 1978a; Armentrout, 1981; Bigelow, 1987; Palmer and Lingley, 1989; Campbell and Nesbitt, 2000). These units currently sit within ~200 m of their original depositional elevation, which implies uplift rates $< \sim 0.05$ m/ky. Slow long-term uplift is also consistent with the preservation of extensive middle and early Pleistocene deposits and constructional landforms along much of the west coast (Thackray and Pazzaglia, 1994; Thackray, 1998, 2001).

Our objective here is to use fluvial terraces to examine the pattern and rates of long-term river incision across the transition from the relatively stable Pacific coast to the actively uplifting interior of the Olympic Mountains. The basic premise is that in well drained landscapes and over sufficiently long spatial and temporal scales ("graded scales" of Schumm and Lichty, 1965), a river will evolve toward a steady-state profile where the rates of river incision and rock uplift are closely balanced along the length of

the river longitudinal profile (long profile for short) (Bull, 1991; Burbank and others, 1996; Maddy, 1997; Pazzaglia, Gardner, and Merritts, 1998; Hovius, 2000). While at steady state, the river maintains its profile and the shape and dimensions of its valley, in the presence of active uplift. This steady-state condition is analogous to what Mackin (1948) called a "graded stream" (see Knox, 1975, and Leopold and Bull, 1979, for further details).

A steady-state profile is an attractive concept because the profile itself could potentially provide a reference for measuring rock uplift, perhaps comparable to using sealevel to measure uplift in coastal areas. However, the stability of this reference frame is not obvious given that river channels are usually constantly adjusting to variations in discharge, sediment load, and uplift. Short-term (< 0.1-1 ky) variations in discharge and sediment yield are usually accommodated at a local scale by changes in channel sinuosity and the position of alluvial bars. Large variations tend to be accommodated over longer time intervals (> 0.1-1 ky) and generally result in drainage-scale changes in the shape of the river profile, including the shape of the associated valley floor.

In tectonically active landscapes, the long-term variations in climate and tectonic forcing are associated with gross changes in the incision/aggradation behavior of the river (Schumm, 1969; Bull, 1991). Typically, these changes occur in a characteristic sequence involving wide incision, aggradation, and narrow incision. (1) *Wide incision* occurs when the river channel incises downward and laterally, commonly into bedrock, to form a broad flat valley bottom. The resulting flat erosion surface is called a strath. (2) *Aggradation* is triggered by an increase in sediment load or a decrease in effective discharge. The valley floor and associated strath surfaces are buried by fluvial sand and gravel, resulting in a fill terrace deposit. Aggradation causes the channel to steepen until it reaches a gradient sufficient to transport the entire sediment load through the river system. (3) *Narrow incision* occurs when the sediment load decreases or discharge increases, causing the river channel to cut downward through the fill terrace deposit and commonly through the underlying bedrock strath as well. Typically, this phase is associated with little to no lateral incision, resulting in a narrow gorge around the active channel. The terrace deposit is abandoned at this stage, leaving behind a record of the incision/aggradation cycle. Continued rock uplift and channel incision cause the terrace deposit to rise above the active channel where it has a greater preservation potential in the hill slopes adjacent to the river.

This interpretation implies a rough connection between bedrock incision and rock uplift. Bedrock incision is determined by measuring the local height of a strath surface above the adjacent modern bedrock channel (assuming that the modern channel is on bedrock). The advantage of this approach is that we are comparing the river under similar hydrologic conditions: the strath was formed when the river was incising into bedrock, and the modern river channel is also incising into bedrock. Furthermore, the wide incision associated with strath formation represents a time when the river was able to maintain a fairly stable long profile, which suggests relatively steady discharge and sediment load. Thus, we propose that the long profile of the river during periods of strath formation was probably similar to the long profile of the modern bedrock channel. This idea is central to many studies that use straths for tectonic interpretation. In our case, we will test this idea by comparing incision rates and erosion rates on different time scales.

Our paper focuses on the Clearwater drainage (fig. 1B), which remained unglaciated during the late Pleistocene and Holocene and thus was able to preserve a flight of fluvial terraces, with the oldest extending back into ~140 ka. An important advantage of the Clearwater is that its main channel has an orientation roughly parallel to the Juan de Fuca-North America convergence direction. We assess how fluvial terraces are formed in this setting and then use features of the terraces to estimate incision rates

along the Clearwater long profile. A simple kinematic model is used to examine the relationship of underplating and frontal accretion to rock uplift and horizontal shortening in the Cascadia forearc high. The long fluvial history preserved in the Clearwater ensures that the unsteady deformation associated with the earthquake cycle is averaged out, leaving us with a record of long-term rock uplift.

TECTONIC SETTING

The Cascadia subduction zone underlies a doubly vergent wedge (*sensu* Koons, 1990, and Willett, Beaumont, and Fullsack, 1993). The change in vergence occurs at the crest of the Coast Range, which represents the forearc high. The doubly vergent system includes a prowedge (or proside) that overrides oceanic lithosphere and accretes turbidites from the deep-sea Cascadia basin and a retrowedge (or retroside) that underlies the east-facing flank of the Coast Range (Willett, 1999; Beaumont, Ellis, and Pfiffner, 1999) (fig. 3). This usage emphasizes the asymmetry of the underlying subduction zone, defined by subduction of the pro-plate (Juan de Fuca) beneath the retro-plate (North America).

Much of the Cascadia forearc high is underlain by the Coast Range terrane, a slab of lower Eocene oceanic crust (Crescent and Siltez formations), which occurs as a landward-dipping unit within the Cascadia wedge (fig. 1A) (Clowes and others, 1987; Parson and others, 1998). Accreted sediments that make up the proside of the wedge reach a thickness of ~15 to 25 km at the present Pacific coast (figs. 1 and 3) and locally extend landward beneath the Coast Range terrane. The Coast Range terrane is clearly involved in subduction-related deformation, although the rate of deformation is relatively slow when compared with the accretionary deformation occurring at the toe of the seaward wedge. Nonetheless, the Cascadia wedge, by definition, includes all rocks that are actively deforming above the Cascadia subduction zone. Thus, the Coast Range terrane cannot be considered a rigid "backstop" but instead represents a fully involved component of the wedge.

Our usage here is at odds with more common usage (Byrne, Wang, and Davis, 1993; von Huene and others, 1998, von Huene, 1998), where wedge deformation is

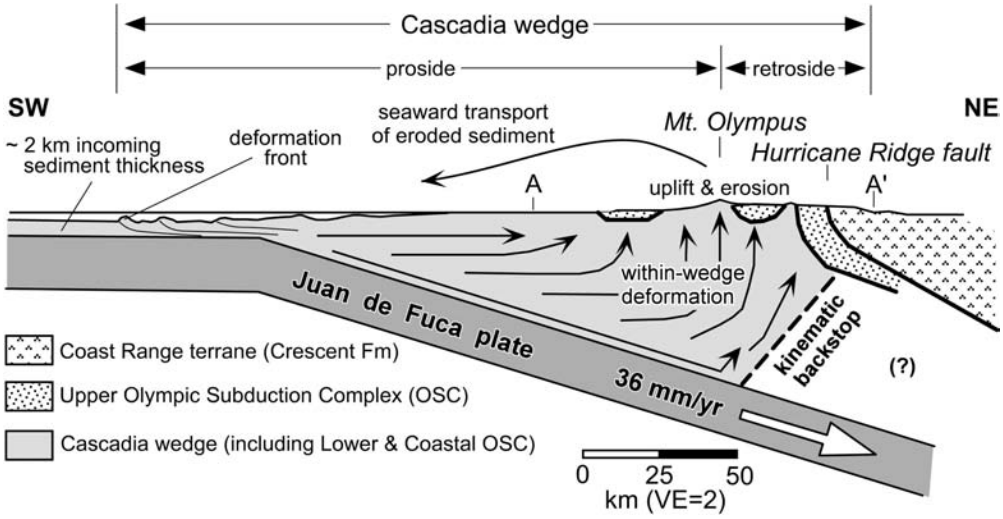

Fig. 3. Schematic section (A-A′ in fig. 1) showing the regional-scale structure of the Cascadia accretionary wedge (after Brandon, Roden-Tice, and Garver, 1998).

viewed as limited to the region seaward of the continental shelf. This alternative view is based on the observation of rapid surface deformation near the toe of the wedge and inferences about the low strength of recently accreted sediments that make up the toe. In this view, the slower surface deformation in the Coast Range makes this area part of the "backstop." There is no support in Coulomb wedge theory for this idea that the limits of the wedge can be defined by surface deformation rates (Beaumont, Ellis, and Pfiffner, 1999). We concur with Koons (1990), Willett, Beaumont, and Fullsack (1993), and Beaumont, Ellis, and Pfiffner (1999) that regional-scale topographic slope provides the best criterion for defining the boundaries of a wedge.

For these same reasons, we avoid the term "accretionary wedge," which carries the implication that deformation is restricted to accreted materials and does not involve upper plate rocks. It has long been recognized that wedge-related deformation in onland collisional orogens commonly involves both accreted materials and older upper plate materials (for example, fig. 1B in Willett, Beaumont, and Fullsack, 1993). Those working at oceanic subduction zones commonly assumed that upper plate rocks would form a rigid backstop because of the inferred lower strength of more seaward accreted sediments (Byrne, Wang, and Davis, 1993; fig. 1A in Willett, Beaumont, and Fullsack, 1993). The involvement of the Coast Range terrane in convergent deformation at the Cascadia margin indicates that this assumption is incorrect.

In the Olympic Mountains, the Coast Range terrane has been uplifted and eroded away, exposing the Hurricane Ridge thrust and the underlying Olympic subduction complex (OSC) (figs. 1 and 3). The OSC is dominated by a relatively competent and homogeneous assemblage of sandstone and mudstone, with minor conglomerate, siltstone, and basalt (Tabor and Cady, 1978a, b). A large part of the OSC was formed by accretion of seafloor turbidites into the proside of the wedge, starting at ~35 Ma (Brandon, Roden-Tice, and Garver, 1998). Where exposed in the Olympics, those accreted sediments are now hard, well-lithified rocks. The steep, rugged topography of the Olympics is supported by both basalts of the Coast Range terrane and accreted sediments of the OSC, which suggests that there is little difference in their frictional strengths (that is, the Coast Range terrane does not have a sufficient contrast in strength to serve as a backstop).

Uplift in the Olympic Mountains has been driven by both accretion and within-wedge deformation (fig. 3) (Brandon and Vance, 1992; Brandon, Roden-Tice, and Garver, 1998). Accretion occurs entirely on the proside of the wedge, resulting in decreasing material velocities toward the rear of the wedge. In the Olympics, retroside deformation is marked by folding of the Coast Range terrane into a large eastward-vergent structure (Tabor and Cady, 1978a, b). The upper limb of that fold, which underlies the eastern flank of the Olympics (fig. 3), is steep and locally overturned. Willett, Beaumont, and Fullsack (1993) show that emergence of a forearc high is commonly accompanied by the development of a large backfold in the retroside of the wedge system (see stage 2 in their fig. 2) in a fashion similar to that observed in the Olympics. We infer from the steep topographic slope on the retroside of the wedge that folding is being driven by a flux of material from the proside of the wedge and that the wedge has not yet begun to advance over the retroside plate (Willett, Beaumont, and Fullsack, 1993).

Brandon and Calderwood (1990) and Brandon, Roden-Tice, and Garver, (1998) argue that deep erosion and high topography in the Olympics are attributed to an arch in the subducting Juan de Fuca plate. This interpretation has been generally viewed with skepticism. Even so, it is well known that the subducting plate is ~10 km shallower beneath the Olympics relative to areas along strike in southwest Washington and southern Vancouver Island (Crossen and Owens, 1987; Brandon and Calderwood, 1990). We do not mean to imply that the topography is dynamically supported by the

arch. Rather, the shallow slab beneath the Olympics means that there is less accommodation space[1] there to hold the growing Cascadia wedge (Brandon, Roden-Tice, and Garver, 1998). This situation plus higher convergence rates and thicker trench fill along the northern Cascadia trench has allowed the Olympics to become the first part of the Cascadia forearc high to rise above sealevel. The early development of subaerial topography plus continued accretion and uplift accounts for the deep erosion observed in the Olympics. The corollary to this interpretation is that adjacent parts of the forearc high will evolve in the same way, although more slowly because of a larger accommodation space for the growing wedge (that is, deeper slab) and slower accretionary fluxes.

REGIONAL GEOMORPHOLOGY

The Olympic Mountains have a broad domal form with the highest elevation and relief centered on Mt. Olympus (fig. 1B). This topography is drained by a radial system of rivers, all originating in the Mt. Olympus area (fig. 1B). A southwest-to-northeast topographic profile across the peninsula reveals a distinct asymmetry with a concave-up pediment on the west side of the range and a dissected plateau-like highland on the east side (fig. 1C). This asymmetry may reflect the fact that storms generally come from the west and that orographically controlled precipitation is focused mainly on the west side of the range (Willett, 1999). Precipitation has a median value of 0.78 m/yr for the peninsula but locally reaches 7.1 m/yr on the western slopes of the range (Daly and Taylor, 1998). Alternatively, the asymmetry may be caused by a non-uniform pattern of uplift.

During the last glacial advance, the Cordilleran ice sheet surrounded the north and east flanks of the Olympic Peninsula (fig. 1B). Geomorphic studies of glacial loading in Puget Sound indicate that areas beyond 35 km from the ice sheet did not experience any significant subsidence (less than ~5 m) during the last glacial advance (see fig. 7 in Thorson, 1989; also geodynamic analysis by James and others, 2000). The Clearwater drainage lies more than 35 km south and east of the margin of the Cordilleran ice sheet (fig. 1B). Thus, glacial loading can be safely ignored in our analysis of long-term uplift there.

Major rivers in the Olympic Mountains generally have smooth concave-up profiles. Local knickpoints are present, particularly in the upper reaches where channel gradients are very steep. All major drainages, with the notable exception of the Clearwater River (Heusser, 1974; Rau, 1975; Thackray, 2001), were extensively and repeatedly glaciated during the Pleistocene (fig. 4A). The continental ice sheet completely overran drainages along the north and east sides of the Olympics. Drainages in the western Olympics were south of the ice margin (fig. 1B) and developed alpine glaciers with equilibrium lines at approx 1200 m elevation (Porter, Pierce, and Hamilton, 1983). The largest alpine glaciers were in the Hoh, Queets, and Quinault drainages where the ice locally advanced all the way to the Pacific coast (fig. 4A) (Heusser, 1974; Rau, 1975; Tabor and Cady, 1978a; Thackray, 1996, 2001). Glaciated drainages generally lack pre-late Pleistocene fluvial deposits and have valleys that are underlain by till, outwash, and lacustrine deposits. Holocene warming has reduced ice cover to ~60 cirque glaciers, located in the headwaters of the Hoh, Queets, Elwha, Dosewallips, and Quinault rivers (fig. 1B).

[1] This term is used in the same way as in basin analysis (Posamentier, Jervey, and Vail, 1988) to mean the maximum amount of space available between the subducting slab and the earth's surface to hold the orogenic wedge. This concept usually assumes isostatic equilibrium and includes subsidence of the lithosphere (that is, subducting slab) caused by the load of the overlying wedge. For example, beneath the center of the Olympic Mountains, there is ~30 km of accommodation space, which includes the mountainous topography (equal to a mean elevation of ~1 km above sealevel).

Fig. 4

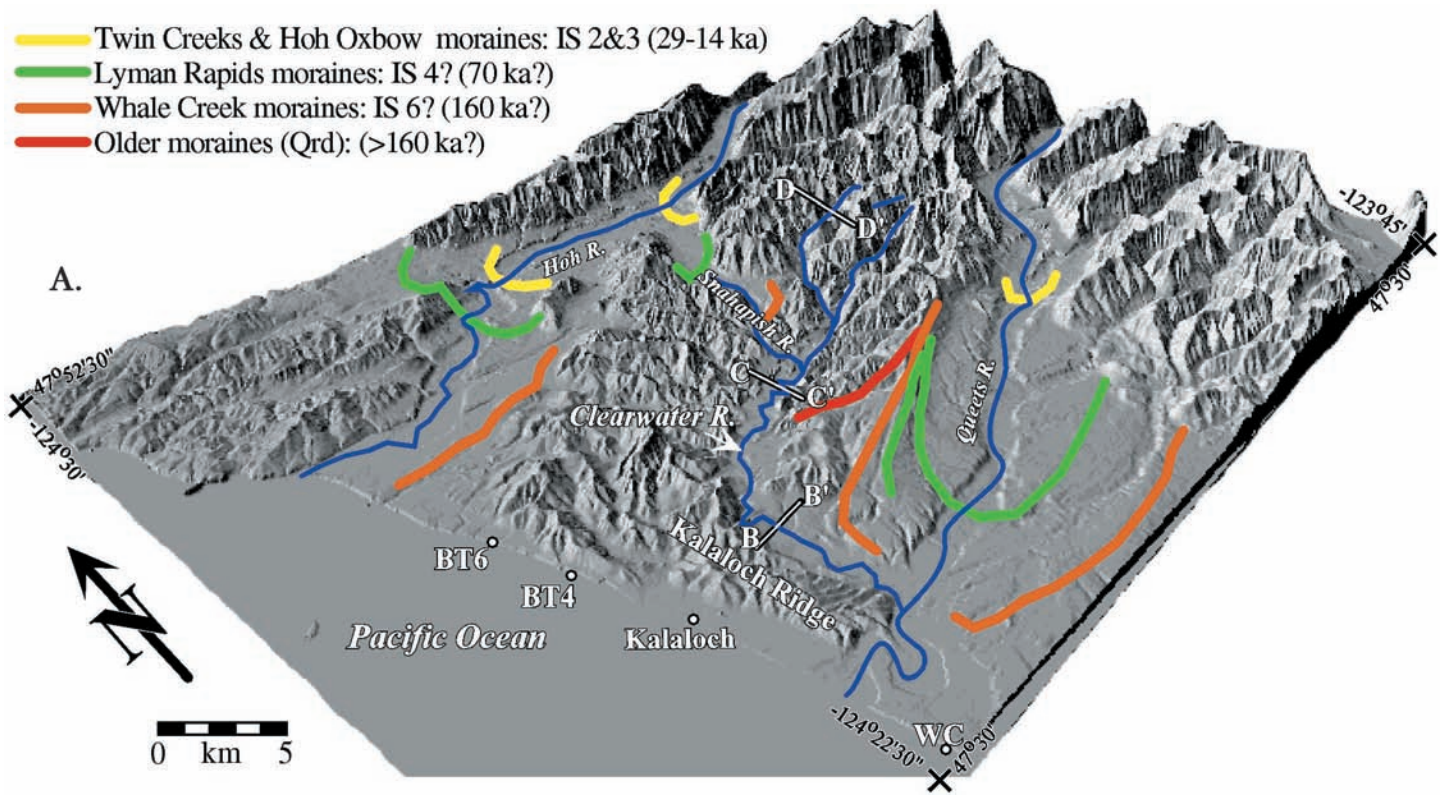

(A) Digital shaded-relief image (30 m-resolution DEM) showing the relation of the Clearwater drainage to adjacent drainages and glacial deposits in the western Olympics (glacial data are from Thackray, 1996, 2001; Easterbrook, 1986). BT6, BT4, and WC mark beach trail 6, beach trail 4, and Whale Creek, where important stratigraphic relationships are exposed along the coast. Profiles B-B′, C-C′, and D-D′ mark cross-valley sections of the Clearwater valley, as presented in figure 8.

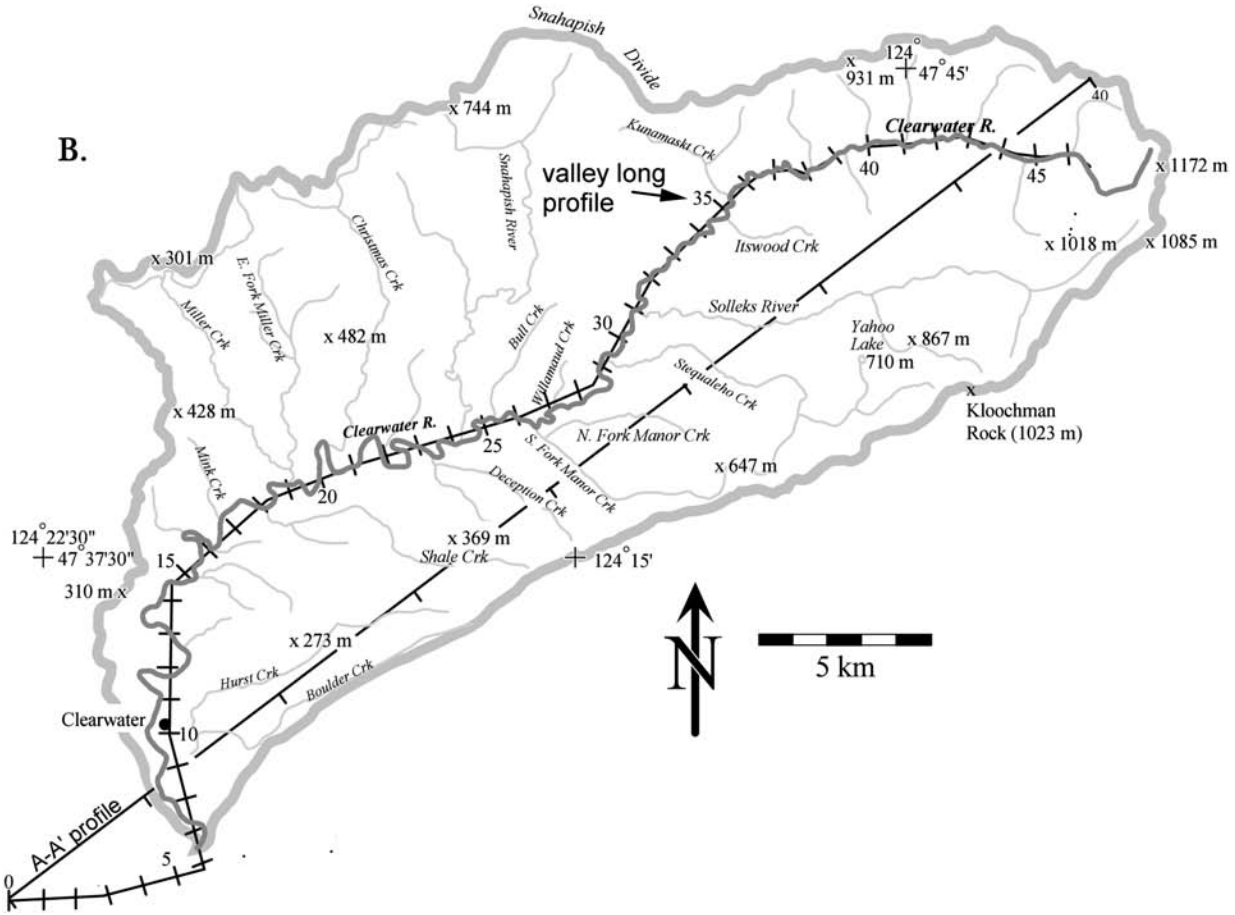

(B) Map of the Clearwater drainage. The valley profile is shown as a crooked thin line with tics marking valley kilometers from the mouth of the Queets River at the coast. The straight section (A-A′ in figs. 1 and 3) is located along the southeast side of the drainage. Final results were projected into A-A′, which parallels the local convergence direction for the Cascadia subduction zone.

Along the west coast of the Olympics, the river channels show little to no incision at the coast, despite the occurrence of significant lowstands (~100 m) during many of the Pleistocene glacial epochs. On first impression, one might expect that a large lowstand would produce an incised channel at the river mouth and an upstream-migrating knickpoint. The subsequent highstand would drown the river mouth and gradually cause any lowstand morphology to be buried by aggrading sediments. However, the lower reaches of the west coast rivers are all presently on bedrock, and they lack any significant knickpoints. We show below that the lack of incision of the Clearwater River during lowstand is because gradients in the lower reach of the Queets valley and across the inner continental shelf are approximately constant. Thus, we suggest that during lowstands, the Queets River was able to extend its mouth across the shelf without appreciable incision or aggradation. Furthermore, we infer that any significant aggradation in the drainage must have been associated with an increase in sediment flux and cannot be attributed solely to changes in sealevel.

Thick constructional terraces are present along most of the west coast. They preserve a clear record of at least two major aggradational events, related to glacially driven increases in sediment flux (Thackray and Pazzaglia, 1994; Thackray, 1998, 2001). The Clearwater drainage remained unglaciated during these events. However, we show below that the lower reach of the Clearwater and Queets valley was deluged by outwash sediment spilling over a low divide (Snahapish River and Christmas Creek) from the Hoh drainage to the north. This enhanced sediment supply caused aggradation of thick terrace sequences in the lower Clearwater River, a relationship that we exploit to constrain the ages of terrace deposits.

CLEARWATER DRAINAGE

The Clearwater drainage covers an area of 390 km^2 and lies between two much larger drainages, the Hoh and Queets (figs. 1B and 4). Elevation in the Clearwater ranges from ~12 m at its confluence with the Queets River to ~1130 m along its eastern divide. Most of the Clearwater is underlain by a rather homogeneous assemblage of medium to coarse sandstone of the Hoh Formation and similar rocks of the Western Olympic lithic assemblage (Tabor and Cady, 1978a). Minor siltstone, mudstone, conglomerate, breccia, and basalt are also present. The relatively uniform bedrock minimizes rock type as a geomorphic variable. There is a precipitation gradient ranging from approx 254 cm/yr at the mouth of the drainage to 400 cm/yr in the headwaters.

We require three schemes to represent distance along the main channel of the Clearwater River. All start at the west coast and include the lower part of the Queets River, which connects the Clearwater River to the ocean. *Channel distance* provides a direct measure of the actual channel length (fig. 5). *Valley distance* is measured along a profile that runs down the central axis of the Clearwater and Queets valleys (figs. 4B and 5). We use this profile to compare projected channel and terrace data. Unless stated otherwise, valley distance is used to describe locations along the river. *Section distance* is measured in a straight profile oriented in the plate convergence direction (A-A′ of figs. 1B and 4B). The A-A′ section is used to interpret the tectonic significance of our results.

The lower Clearwater River extends from its confluence with the Queets at km 6, to its confluence with the Solleks River at km 31. This reach has a mixed bedrock-alluvial channel, which meanders through a 1 to 2 km-wide, low-relief valley (fig. 4). Nowhere is the channel far from bedrock, even where it empties into the Queets River. To confirm this point, we checked drilling logs for the Clearwater-Snahapish Road bridge, located near the confluence of the Clearwater and Queets rivers, and the Highway 101 bridge across the Queets, which lies about 1 km from the mouth of the

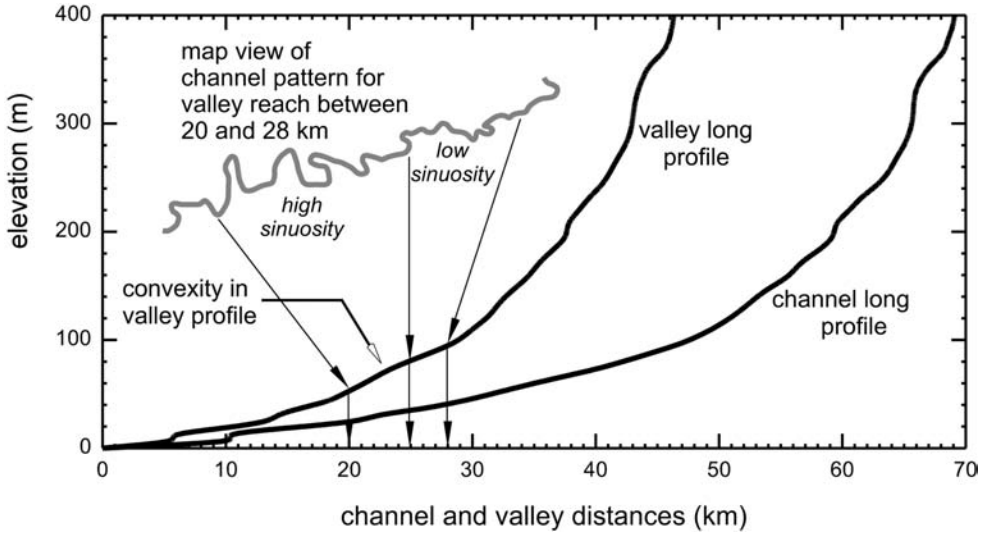

Fig. 5. Plots of the valley and channel long profiles for the Clearwater River. See text for discussion of convexity in the valley profile between km 20 and 28.

river (Washington State Department of Transportation Geotechnical Report, 1988). The alluvial cover was everywhere < 5 m. No alluvial-filled inner channel was found. The valley gradient is 0.0033 (rise over run), and the channel sinuosity is 1.66 (channel length over valley length). The most sinuous segment of the Clearwater River lies in this lower reach, between km 20 and 24 (figs. 4B and 5). The upper Clearwater River (above km 31) has a channel cut mainly in bedrock. Here, the valley gradient is steeper (0.0167), and the sinuosity is lower (1.15).

The drainage divide between the Clearwater and Hoh rivers has two low-standing segments at the heads of the Snahapish River and Christmas Creek (fig. 4B). The larger segment, ~2 km long, lies at the head of the Snahapish valley, where it stands only 50 m above the adjacent valley floors. As shown in figure 4A, the Snahapish divide is underlain by the Lyman Rapids and Whale Creek moraines, which formed during major glacial advances in the Hoh drainage. These units (dated elsewhere, not in the Snahapish valley) are >47 ka (radiocarbon dead). Thackray (1998, 2001) tentatively assigns these moraines to glacial epochs during marine oxygen isotope stages (IS) 4 and 6 (fig. 6). We present evidence below that supports this assignment. A set of younger moraines, Twin Creeks and Hoh Oxbow (fig. 4A), formed at 29 to 14 ka (fig. 6), during the last glacial maximum (Thackray, 1998, 2001). Their internal position relative to the older moraines (fig. 4A) indicates that this last glacial advance and its outwash did not reach and overtop the Snahapish divide.

The modern Snahapish River is underfit; it is too small to have cut its valley. The valley itself is choked by a thick fill of glacio-fluvial outwash that grades into heads of outwash. These deposits are clearly genetically related to glacial advances in the Hoh drainage during Lyman Rapids and Whale Creek times. The Snahapish valley and, to a lesser degree, the Christmas Creek valley acted as conduits for outwash moving from the Hoh drainage into the lower part of the Clearwater drainage. We show below that this bypassing of sediment had a strong influence on fluvial aggradation in the lower reaches of the Clearwater and Queets rivers.

Mapping corroborates the dominance of fluvial and hillslope deposits and the subordinance of glacial deposits in the Clearwater drainage. The only direct evidence

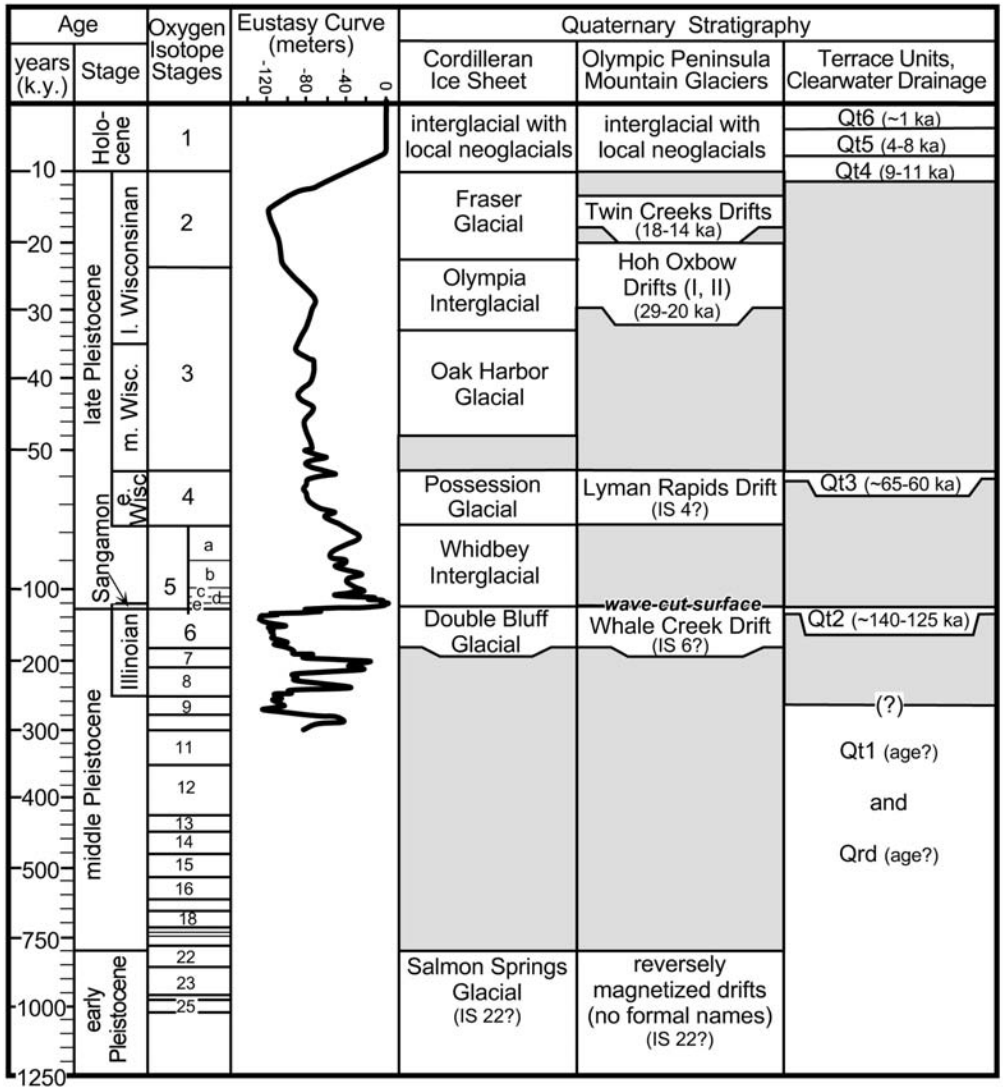

Fig. 6. Regional stratigraphic correlations for glacial and fluvial deposits in the western Olympic Peninsula and surrounding regions. Note the variable scaling in the time axis. Eustasy curve is from Chappell and others (1996) for 0 to 140 ka, and Pillans, Chappell, and Naish (1998) for 140 to 300 ka. The next column shows deposits associated with advances and retreats of the Cordilleran ice sheet in Puget Sound, as synthesized by Easterbrook (1986). The next column shows the stratigraphic record of alpine glaciation in the western Olympics, based on the work of Thackray (1996, 2001) We have excluded his drift unit, called Oxbox Ø and estimated to be 39 to 37 ka, because it is based solely on an isolated sequence of lake sediments. The final column shows terrace stratigraphy in the Clearwater valley as determined by work presented here.

for ice in the drainage is in the form of radiocarbon-dead lacustrine deposits overlying a lodgment till (Wegmann, 1999) near km 42. There are several waterfalls on tributary channels upstream of this point, consistent with glacially-produced hanging valleys, but the overall morphology of the main valley shows no significant evidence of alpine glaciation.

Interfluves and hillslopes are mantled with poorly-stratified, poorly-sorted colluvial deposits, <1 to 6 m thick. These deposits are variably weathered, which is reflected

in their color (recorded as hue, value, and chroma with a Munsell soil color chart) and clast-to-matrix ratio. Relatively unweathered colluvium tends to be clast-supported with brownish (10YR hues) coloration, whereas more weathered colluvium is generally matrix-supported, in that it contains more pedogenic clay, with yellow, red, and orange (5YR - 7.5YR) coloration. The degree of weathering in all Clearwater hillslope or alluvial deposits increases with relative stratigraphic age. This relationship is quantified below using clast weathering rinds. Buried colluvium is locally present in the middle of the Clearwater drainage and becomes increasingly abundant in the upper part of the drainage, where it is interbedded with alluvial fan deposits. Buried colluvial/alluvial fan deposits are distinguished by a relatively high percentage of locally-derived angular clasts, including fragile shale clasts.

FLUVIAL STRATIGRAPHY OF THE CLEARWATER VALLEY

Overview.—In actively rising landscapes, river valleys will commonly contain a record of past valley bottoms, preserved as terraces on the valley slopes above the active river channel. Unconformities are used to divide terrace deposits into mapable allostratigraphic units. The bedrock unconformity at the base of the terrace deposit is called a strath, and the uppermost constructional surface of the deposit, a tread.

We distinguish between two different types of mapable terrace deposits. A fill terrace deposit is a thick deposit of alluvium, resting on a strath, and usually formed by widespread aggradation along the length of the river (Bull, 1991, p. 8). In contrast, a strath terrace deposit describes a thin layer of alluvium resting on a strath surface and represents the bedload that was left behind by the active river channel. For practical purposes, a unit is assigned as a strath terrace deposit where it has less than 3 m of coarse alluvial sediment, which represents the approximate scour depth and characteristic bedload thickness that could be mobilized during bankfull discharge in a river the size of the Clearwater. Geologically speaking, the cutting of a strath and deposition of an overlying strath terrace unit occur at the same time because the moving bedload is what abrades the strath. On the other hand, a fill terrace deposit may take up to 10 ky to accumulate (Weldon, 1986). Thus, the fill provides only a minimum age for burial of the underlying strath surface.

The valley walls of the Clearwater drainage contain a series of paired and unpaired terrace deposits inset into the valley walls at 1 to 110 m above the modern channel (figs. 7 and 8). The river valley and adjacent terraces show marked changes in an upstream direction (fig. 7). The lower reach of the Clearwater (cross-valley sections B-B′ and C-C′ in fig. 8) is flanked by low well-rounded interfluves. The terrace deposits are made up of 5 to 40 m of coarse, stratified sand and gravel and sit on straths 0 to 20 m above the elevation of the modern valley bottom. Locally, the fill has buried not only the paleo-valley bottom (equivalent to the strath) but also the side slopes of the river valley itself (for example, Qt2 in C-C′ in fig. 8), thus forming a buttress unconformity. Sedimentary structures within the terrace deposits include broad, shallow channel forms exhibiting 0.5 to 2 m-high tabular cross beds, and smaller-scale trough crossbeds in finer-grained silty-sand beds. This sedimentology is generally consistent with a braided channel pattern and mimics the features exhibited by glacio-fluvial deposits that can be physically traced to heads of outwash in adjacent, glaciated drainages. The terrace alluvium is capped by about 1 to 2 m of thin-bedded sand, locally laminated silt, and massive silt, which are interpreted as overbank and loess deposits.

The upper reach of the Clearwater is characterized by a narrow V-shaped gorge, which lies inside a wider V-shaped valley (D-D′ in fig. 8). The fill terraces that characterize the lower reach give way to unpaired strath terraces in the upper reach. Locally, pediment gravel and thin alluvial fan deposits mantle the slopes of an outer valley and grade into the highest strath terraces, which lie at the break in slope between

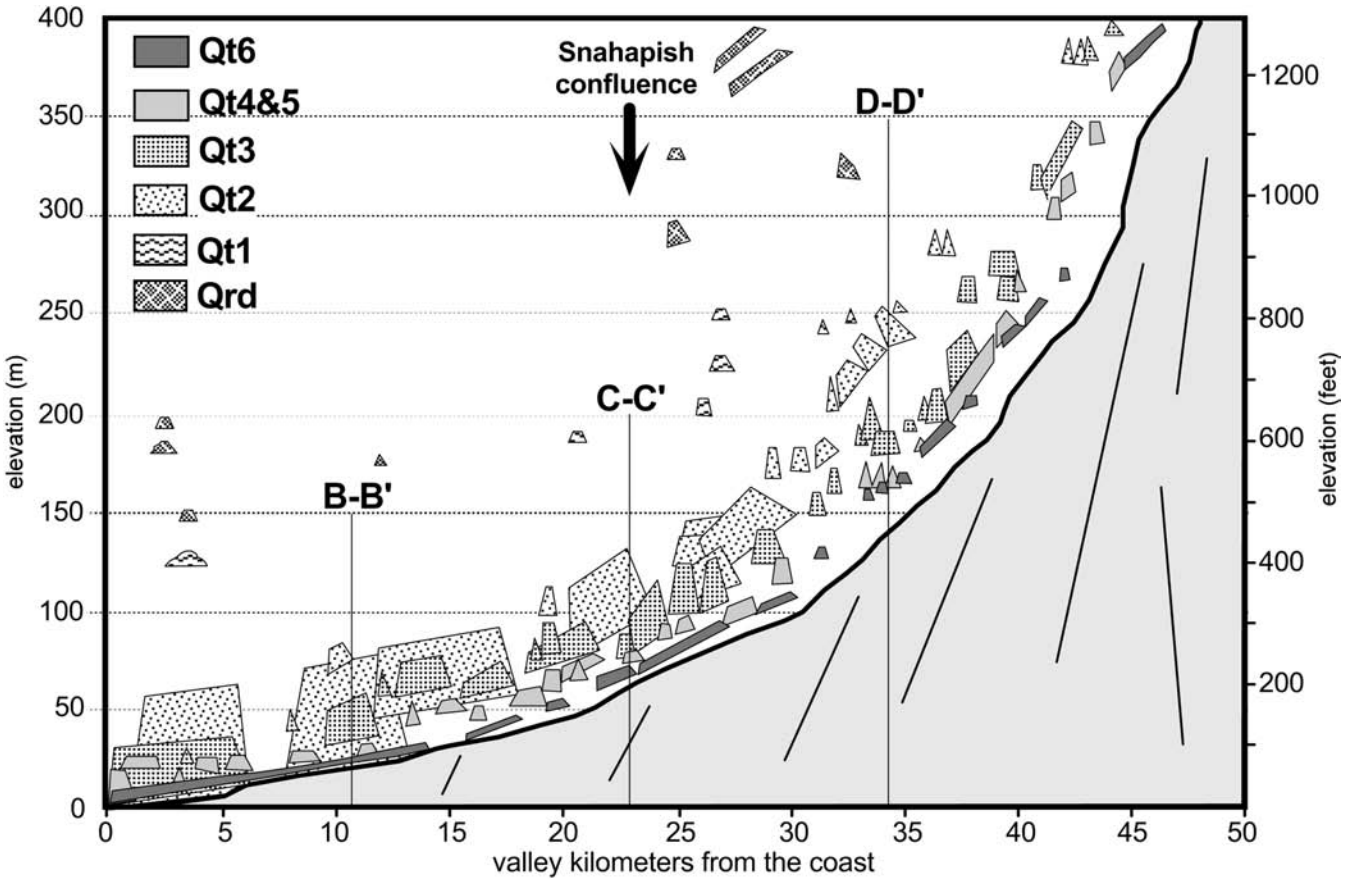

Fig. 7. A long-profile section of the Clearwater valley showing the vertical relationship of mapped terrace deposits (polygons) to the modern Clearwater River (continuous line). Terrace units were projected orthogonally into the valley profile from their mapped positions along the flanks of the Clearwater valley (fig. 4B). The bottom and top of each polygon corresponds to the strath and tread, respectively, for a mapped terrace deposit.

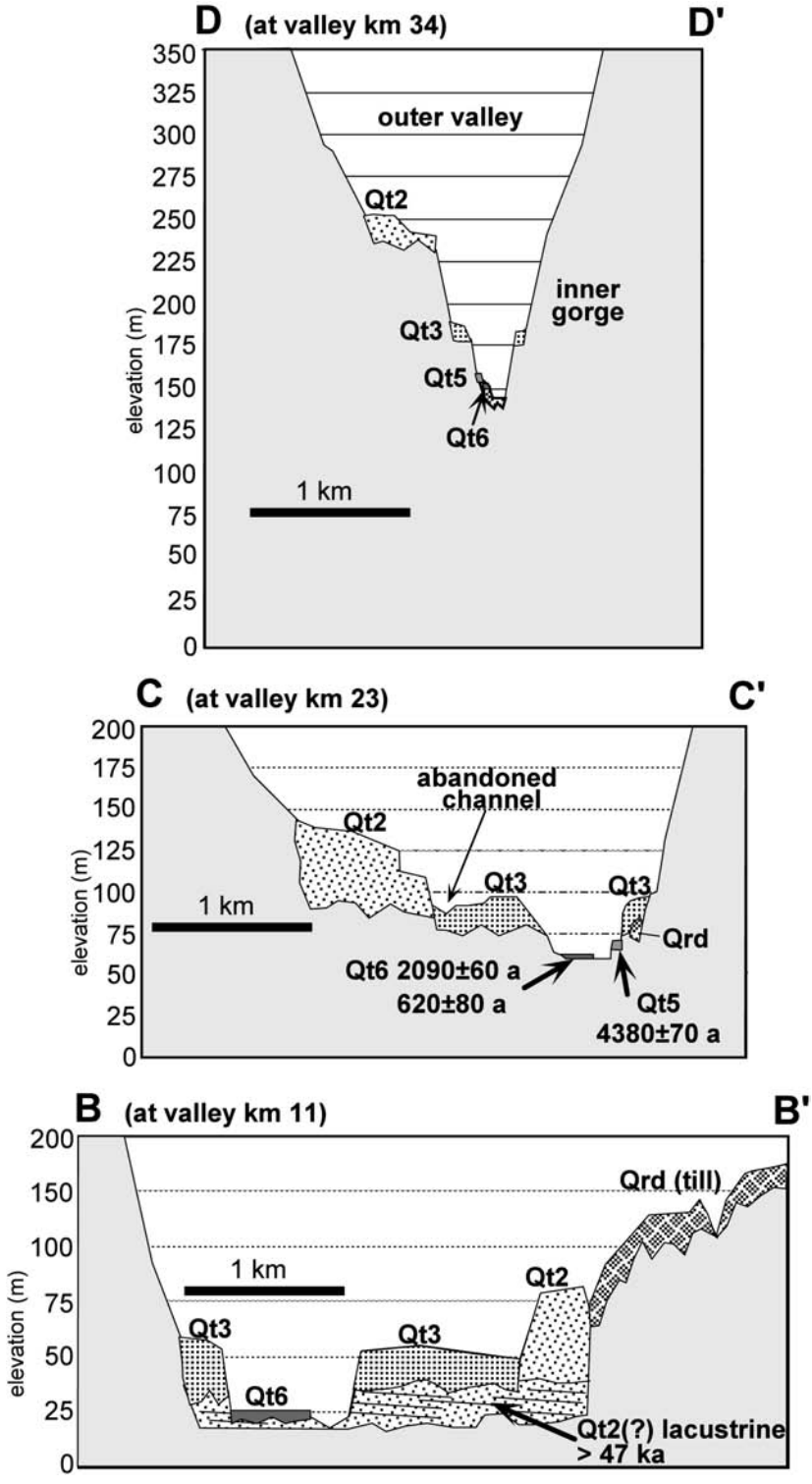

Fig. 8. Cross-valley profiles of the lower (B-B′), middle (C-C′), and upper (D-D′) parts of the Clearwater valley showing the relationship of the terrace units to the local valley geometry. Locations are shown in figure 4A.

the outer valley and an inner valley gorge. Upstream from Kunamaskt Creek (fig. 4B; D-D′ in fig. 8), all of the terraces are strath terraces, cut into pre-Quaternary bedrock or old Quaternary deposits (units Qt1 or Qrd, defined below).

Mapping and relative ages.—We have identified six terraces, Qt1 to Qt6, based on a 1:12,000 scale surficial geologic map of the Clearwater watershed. Our mapping considered relative stratigraphic position, elevation of the terrace base above the modern stream (fig. 7), character of the soil profile developed in the terrace tread (table 1), and correlations with other Quaternary deposits in adjacent drainages and at the Pacific coast (Thackray, 1996; Wegmann, 1999). Much of the terrace correlation, including the link between upstream strath terraces and downstream alluvial fills, is well defined by these basic map relations. All terrace units are described here, but we are especially interested in the largest and most continuous units, Qt2 and Qt3, which are used to estimate fluvial incision along the trunk of the Clearwater River.

Soil profile development and clast weathering rinds (figs. 9 and 10; table 1) in the terrace treads provide additional controls in distinguishing between deposits of different age and linking upstream and downstream remnants of the terraces. Soil descriptions and terminology follow the United States Department of Agriculture Soil Taxonomy (Soil Survey Staff, 1975). For the rind-thickness methods, we follow procedures outlined in Chinn (1981), Knuepfer (1988), McSaveney (1992), and Ricker, Chinn, and McSaveney (1993). Rinds were measured to the nearest 1 mm on clasts of graywacke sandstone that were about 4 to 10 cm in diameter and had well-defined concentric rinds and unweathered cores. Most weathering rind studies sample clasts from the surface of the terrace, but this is not possible in the wet and heavily vegetated Clearwater drainage. Good exposures of terrace treads are only

TABLE 1

Summary of terrace units

Terrace unit	Parent material	Tread elev. at coast (m)	B horizon color	Depth of oxidation (m)	Mode of rind thickness (cm)	Age of deposit	Inferred age of strath
Qt6	stratified fluvial sand, silt, clay	< 5	brown (10 YR)	1 – 2	0 - 0.2	1 ka*	late Holocene
Qt4 and Qt5	stratified fluvial sandy gravel with a silt-dominated overbank cap	5-10	yellowish-brown (10 YR)	2 – 3	0.3 – 0.4	4 – 8 ka * and 9 – 11 ka*	early Holocene and latest Pleistocene
Qt3a and Qt3b	stratified fluvial sandy gravel with a loess-dominated cap	30	yellow (10YR – 7.5YR)	4 – 5	0.3 - 0.4	~65 – 60 ka	~65±20 ka, late Pleistocene, IS 4
Qt2a through Qt2d	stratified fluvial sandy gravel with a loess-dominated cap	60	brownish-red (5 YR – 7.5YR)	~10	0.9 – 1.2	~140 – 125 ka	~140±20 ka, late middle Pleistocene, IS 6
Qt1 and Qrd	mostly roundstone diamicton	> 60	brownish-red and red (2.5 YR – 5YR – 7.5YR)	> 5 – ?	> 2	> 200? ka	middle Pleistocene?

* = precise age control provided by a subset of approx 55 radiocarbon AMS dates (Wegmann, 1999; Wegmann and Pazzaglia, submitted).

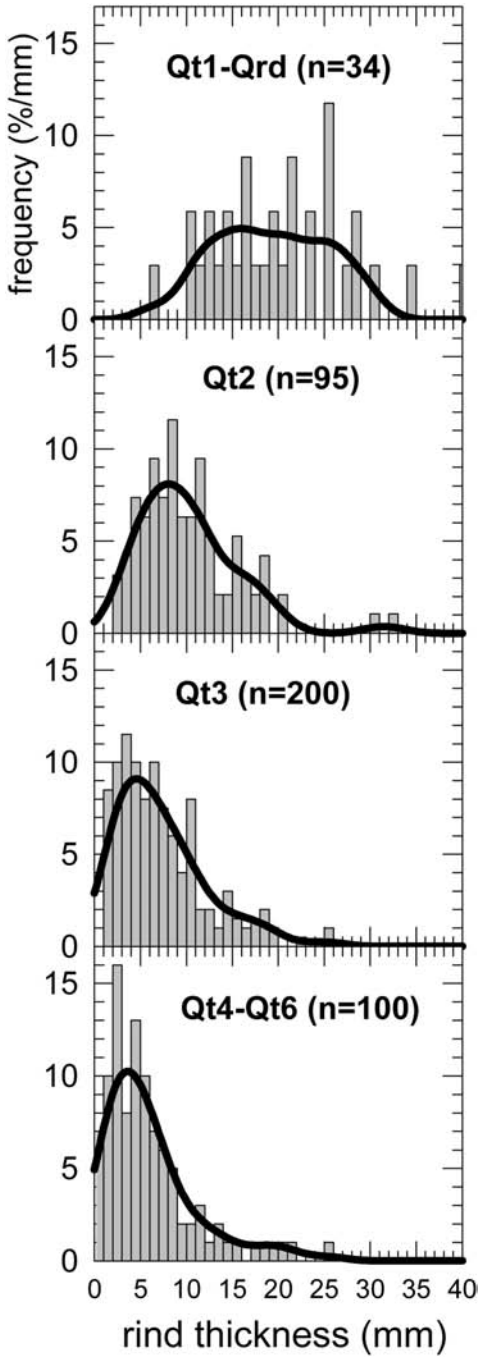

Fig. 9. Thickness distributions for clast weathering rinds for terrace deposits of different stratigraphic age. The probability density curves were calculated using the Gaussian kernel method (Brandon, 1996), with the kernel size set to 2 mm. Qt1 to Qrd is from an interfluve at ~180 m elevation on the north divide of Shale Creek. Qt2 is from the Peterson Creek terrace at ~130 m elevation. Qt3 is from the Quinault quarry pit at ~30 m elevation. Qt6 is from an exposed gravel bar adjacent to the Clearwater River, near the Clearwater picnic area, ~2 km south of the town of Clearwater.

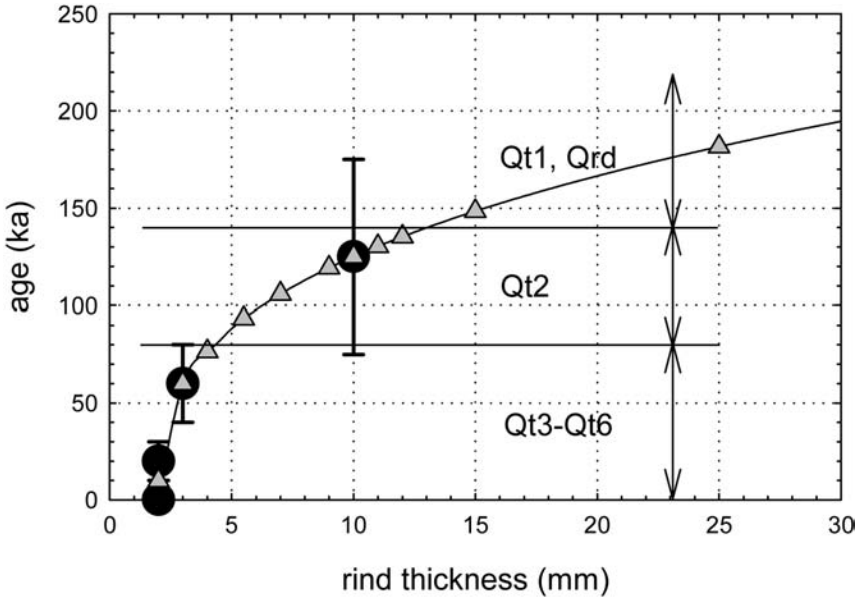

Fig. 10. Rind-thickness data for graywacke clasts at various sample localities in the terrace units. The average thickness at each locality is represented by the mode of the density plot (fig. 9). Four calibration points (solid circles with estimated 2SE error bars) from localities with well-constrained ages were used to define a best-fit curve, using an offset power function with a form: $\tau = A(T\text{-}T_0)^B$, where τ is age in ka, and T is thickness in mm. The fit parameters were determined by least-squares: $A = 59.86$, $B = 0.354$, and $T_0 = 2.0$. Rind-thickness modes from undated terrace units (gray triangles) are plotted using ages predicted by the calibration curve.

available in gravel-pit highwalls and a few road cuts. Otherwise, the treads are either densely forested with no clasts exposed at the surface, or they are significantly disturbed by logging.

We avoided this problem by sampling buried clasts collected from a defined position with the terrace soil profile (Colman and Pierce, 1981, 1986). We expect that clasts buried in the soil profile should weather in the same manner as those at the surface. The soil profile lies within the upper 3 m of the terrace and thus is relatively thin compared to the thickness of the overall deposit, which might reach some 30 m or more. Furthermore, clasts at the surface and in the soil profile are subjected to similar wet-dry cycles, associated with infiltration of precipitation and fluctuations of the groundwater table.

Sampling was done in high-wall gravel pits, which provide large cross sections, tens of meters in length, of the terrace treads. These exposures show that the soil profiles have been intensely bioturbated down to a depth of at least a meter, and in some cases more, including most of the B horizon of the soil profile. Clasts were collected from the base of the B horizon, where they generally preserve their original depositional fabric, indicating minimal bioturbation. Terrace treads commonly have a fine-grained cap composed of fluvial or eolian sediment. Field and airphoto observations show that soil drainage is poor in areas where this fine-grained cap is thick. In our sampling, we selected areas that were well drained (that is, minimal fine-grained cap) in order to avoid the influence of variable soil drainage on the degree of clast weathering.

Figure 9 shows that the younger deposits tend to have tight unimodal rind-thickness distributions, with a long tail on the high side of the distribution, whereas the older deposits show broader, more-symmetric distributions. Modes were used as the

representative thickness, as recommended by McSaveney (1992). Four localities have suitable age control to be used as calibration points (large circles in fig. 10). An approximate age-thickness curve was estimated using an offset power function (modified from Chinn, 1981). The triangle symbols (fig. 10) show predicted ages for rind-thickness modes for undated terrace units.

We caution against putting too much reliance on specific age estimates or our determination of an age-thickness curve. What is more important is that the terrace units show a clear trend of progressively thicker rinds with increasing stratigraphic age. This result represents a positive test of our abilities to map, correlate, and sequence the terrace deposits according to their relative age.

Stratigraphic units.—Qt6 is the youngest terrace unit and is characterized by brown (10YR), poorly developed soils, rind-thickness modes between 0 and 2 mm, and an oxidation depth of 1 to 2 m in pebbly and sandy silt deposits. Soils are developed mainly in fine-grained overbank deposits with little to no illuviated material in the underlying sand and gravel. Soil profiles typically consist of a 20 cm-thick A horizon, a 30 cm-thick cambic B horizon, and a thin oxidized C horizon 1 to 3 m thick. Qt6 fills are thickest, reaching a maximum of 4 m near the mouth of the Clearwater and thinning considerably upstream. They become strath terrace deposits at about km 35. The strath surfaces beneath Qt6 lie within ~2 m of the modern river channel and have gradients similar to the modern channel.

Qt5 and Qt4 have poorly-developed brown and yellow-brown soils. Rind-thickness modes are between 3 and 4 mm, and oxidation extends to ~2 to 3 m depth, and locally >4 m in coarse alluvium. Post-depositional modification is minor on the terrace treads, which retain a constructional morphology with well-preserved overbank deposits and local loess. A typical soil profile exhibits a 50 cm-thick B horizon composed of yellowish brown (10YR) silt loam to silty clay. Qt5 and Qt4 are best preserved below km 35. Their straths sit at a consistent height of ~3 to 5 m above the modern channel, and their treads, at a height of ~5 to 10 m.

Qt3 has a moderately developed yellow soil profile, rind-thickness modes between 3 and 4 mm, and an oxidation depth of 4 to 5 m, but locally ~10 m in coarse alluvium. Post-depositional modification is minimal on the terrace treads, which retain a constructional morphology with well-preserved sandy overbank and silty loess deposits. The loess is >1 m near the Snahapish River and the coast. Soil profiles consist of a 50 to 80 cm-thick B horizon composed of yellowish brown (10YR) to brown (10YR-7.5YR) silt loam with numerous thin clay films preserved on soil ped faces. Soil profiles in fine-grained material have strong brown colors (7.5YR) and well-developed soil structure. Qt3 is best preserved below about km 24, where it locally has two treads, designated as Qt3a and Qt3b, with the Qt3b tread sitting about ~4 m below the Qt3a tread. In this part of the valley, Qt3 straths maintain a gentle gradient, lying 6 to 10 m above the channel, and treads are ~35 m above the channel. Above km 24, Qt3 has only one tread, and the straths take on a steeper gradient, climbing to a maximum height of ~70 m above the channel.

Qt2 deposits have well-developed brownish-red colored polygenetic soils. Rind-thickness modes are between 9 and 12 mm, and the oxidation depth is ~10 m in coarse sand and gravel. There are 4 distinct treads associated with the Qt2 fill, especially in the region surrounding the Snahapish-Clearwater confluence. The treads are named Qt2a through Qt2d, in order of decreasing elevation and age of the tread. All these treads show significant post-depositional modification caused by root bioturbation and colluviation, as well as multiple episodes of loess deposition. Morphology and soil stratigraphy vary on the treads, with well-developed soils on well-drained colluviated slopes and more poorly developed, loess-rich soils on eroded interfluves. In the low-relief, stable parts of the tread, soils consist of a 10 cm-thick A horizon, a local 1 to

10 cm-thick albic horizon, and a 50 to 100 cm-thick B horizon composed of brown (7.5YR) and strong brown (7.5YR) clay loam with moderately thick clay films. Along the lower Clearwater, the Qt2 strath sits at 15 to 40 m above the modern channel, and the oldest tread, Qt2a, sits at ~60 m above the channel. In the upper Clearwater, the Qt2 strath takes on a steeper gradient, rising to a maximum of ~110 m above the modern channel in the uppermost part of the drainage.

The primary tread, Qt2a, marks the constructional top of the original fill unit. The next three treads, Qt2b,c,d, mark a series of unpaired fill-cut terraces inset into the primary deposit. These minor inset units are thought to have formed during a series of local events within the river ("complex-response" terraces of Schumm, 1973; Bull, 1991, p. 24 - 25) during incision of the Qt2 fill. In contrast, the continuity and paired geometry of the other terrace treads, most notably Qt2a and Qt3a, indicate they were formed by events that affected the entire drainage.

The oldest Quaternary units in the Clearwater, Qt1 and Qrd, are restricted to isolated outcrops along the crest of some high-standing interfluves. These units have similar weathering characteristics but different sedimentology and origins. Qt1 is interpreted to be strictly fluvial in origin, based on its more stratified character and its relationship to the modern Clearwater channel. If correct, it may be the oldest and most deeply incised terrace fill in the Clearwater drainage. Qt1 crops out in the center of the drainage, where it lies >100 m above the modern channel. It consists of weakly stratified, highly dissected and colluviated fluvial sand and gravel. Clasts are generally well rounded and highly saprolitized. Those that preserve weathering rinds have a modal thickness >20 mm. Qt1 soils are complex and polygenetic and have multiple 1 to 2 m-thick truncated B horizons composed of strong brown (7.5YR), reddish-brown (5YR), and red (2.5YR) clay-rich soil.

Qrd consists of poorly sorted, unstratified sand, and matrix-supported gravel. The unit is interpreted to be a relatively old glacial or glacial-fluvial deposit. Deposits include some deeply weathered tills exposed along the crest of Kalaloch Ridge (fig. 4A), and at the top of the interfluves between Willamaud and Bull creeks and Shale and Deception creeks (fig. 4B). These deposits are considered to have formed during glacial advances from the adjacent Queets and Hoh drainages (Queets glaciation on the southeast side of the Clearwater drainage; Hoh glaciation for the area between Snahapish River and Bull Creek, and along Kalaloch Ridge from Kalaloch to Snahapish River divide; for details, see Heusser, 1974; Rau, 1975; Thackray and Pazzaglia, 1994; Thackray, 1996).

Weathered till and lacustrine deposits (Qrd) locally crop out in the valley bottom above km 42 (fig. 4B; Wegmann, 1999). In the headwater of the Clearwater (above km 45), several distinct flat surfaces are preserved high on the valley walls. These surfaces are locally underlain by a dark gray diamicton with angular clasts. There are no direct ages for these deposits, but deep weathering suggests that they are some of the oldest surficial deposits in the drainage.

Age of terrace units.—Qt4, Qt5, and Qt6 are all Holocene to latest Pleistocene in age (0 - 11 ka in fig. 6). The detailed age data for these units come from approx 55 radiocarbon AMS dates presented in Wegmann (1999) and Wegmann and Pazzaglia (submitted). The older terraces are all pre-Holocene in age. Numerous organic samples from Qt3 have consistently given "radiocarbon dead" results, indicating an age > 47 ka (Heusser, 1972; Florer, 1972; Thackray, 1996, 2001). We have recovered well-preserved wood from laminated lacustrine beds interbedded with Qt2 fluvial deposits (B-B′ in fig. 8). It too was radiocarbon dead (> 47 ka, Beta 75762).

We can infer specific ages for the Qt2 and Qt3 deposits by correlations to glacial stratigraphy in the Hoh and Queets drainages (Thackray, 1996, 2001) and eustastically controlled stratigraphic relationships preserved at the coast. In estimating ages, we

focus on the main part of the fill deposit, which is defined to lie below the oldest tread in each deposit (Qt2a and Qt3a). These deposits are the oldest and mark when the underlying strath was buried, so their ages are important for our estimation of incision rates for the Qt2 and Qt3 straths.

The coastal sequence and related deposits have been studied in considerable detail (Crandell, 1964, 1965; Huesser, 1964, 1972, 1973, 1974, 1978; Moore, 1965; Florer, 1972; Rau, 1973; Easterbrook, 1986; Saunders, Clague, and Roberts, 1987; Thackray and Pazzaglia, 1994; Thackray, 1996, 1998, 2001). The sequence is dominated by two glacio-fluvial fan-delta sequences that were fed by outwash from point sources at the mouths of the Hoh and Queets rivers. The outwash can be physically traced to terminal moraines in the Hoh valley that mark the limits of major alpine glacial advances in the upper Hoh (fig. 4A). Recall that the Lyman Rapids and Whale Creek advances in the Hoh valley were of sufficient magnitude to breach the low divide west of the Snahapish River (fig. 4A). The thick fill terraces, Qt2 and Qt3, mark the two times that outwash from the Hoh spilled into the lower Clearwater valley. We infer that during each of these events, the Clearwater River was initially unable to transport the increased sediment flux. The result was widespread deposition in the lower parts of the Clearwater and Queets valleys and outward across the exposed continental shelf. Deposition continued until the river profile was steep enough to transport the enhanced sediment load.

The Qt2a and Qt3a terrace treads can be physically traced, unbroken for over 5 km, from the mouth of the Clearwater, down through the lower Queets valley and to the coast where they merge with well formed treads marking the tops of two coastal aggradational sequences (fig. 11) (Thackray and Pazzaglia, 1994; Thackray, 1996). Remnants of these coastal deposits can be found on sea stacks and small islands up to 6 km offshore (for example, p. 19 in Rau, 1973). The two aggradational units at the coast are separated by a widespread wave-cut unconformity that is typically assigned to the Sangamon highstand at ~122 ka during IS 5e (Rau, 1973; Thackray and Pazzaglia, 1994; McCrory, 1996, 1997; Thackray, 1996, 1998) (figs. 6 and 11). The Sangamon

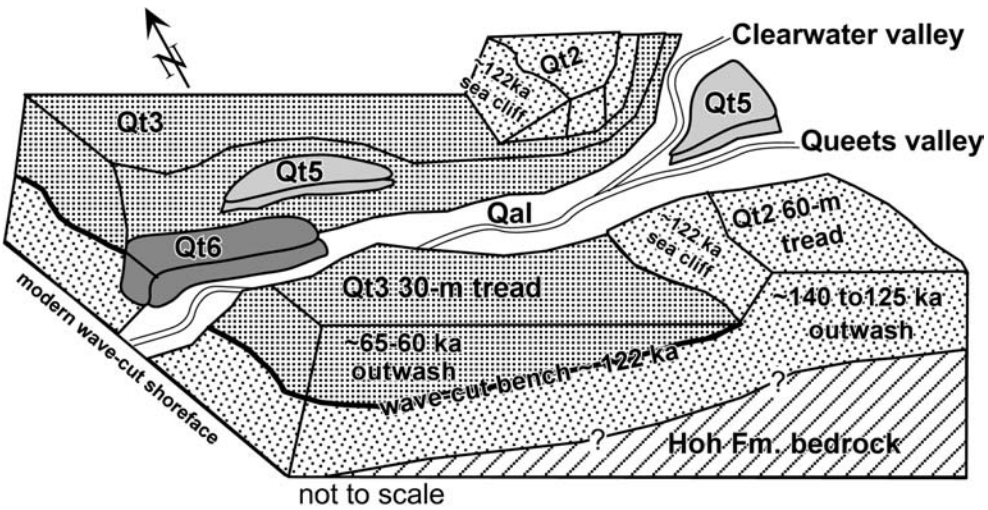

Fig. 11. Correlation of constructional glacio-fluvial terraces at the coast (Thackray, 1996, 2001) to fluvial terraces in the lower parts of the Queets and Clearwater drainages. The coastal stratigraphy is used for age control in the Clearwater drainage. See text for details.

high marks the highest stand of sealevel in the past ~250 ka (fig. 11), reaching +5 ± 2 m amsl at 122 ± 4 ka (Muhs, 1992; Chappell and others, 1996).

Lajoie (1986) and Anderson, Densmore, and Ellis (1999) report examples where marine-terrace cutting occurred at IS 5a (~85 ka) and not IS 5e, but they argue that this result occurs where a coastline is being rapidly uplifted, as indicated by preservations of flights of wave-cut terraces. As discussed earlier, long-term uplift along the Olympic coast has been very slow (for example, flights of wave-cut terraces are notably absent). Thus, for the Olympic coast, the highest wavecut terrace should correspond to the highest stand of sealevel, which is the Sangamon highstand. Thackray (1998) discusses the possibility that the wavecut terrace was cut at IS 5c or IS 5a (105 or 85 ka, respectively), but we consider these options untenable given that sealevel was some 25 to 30 m lower than the Sangamon highstand (fig. 6).

The wavecut origin of the unconformity is indicated by a thin beach deposit with marine fossils lying directly above the unconformity. Glacio-fluvial deposits below the unconformity are correlative with Qt2 (fig. 11). The Qt2a tread is cut out at the coast by the unconformity, but it is exposed ~1500 m inland as a distinct flat surface at ~60 m above modern sealevel (amsl) (Thackray, 1996). It is this terrace tread that can be traced back to Qt2a in the Clearwater drainage. At the coast, glacio-fluvial deposits above the unconformity are correlative to Qt3. The terrace tread for this deposit is at an elevation ~30 m amsl at the coast and is coextensive with the Qt3a terrace tread in the Clearwater valley. Numerous organic samples from these coastal units have yielded radiocarbon-dead results (Heusser, 1972; Florer, 1972; Thackray, 1996, 2001). From this, we conclude that Qt3 is older than ~47 ka but younger than the ~122 ka unconformity, and Qt2 is > 122 ka (fig. 6).

We can refine these age estimates by examining the relationship of the Qt2a and Qt3a aggradational events to global eustasy. Figure 12 shows the valley profile and valley gradient in the Clearwater-Queets drainage and its continuation across the continental shelf. We focus on the valley long-profile because we have no information about the channel long profile for the offshore area nor do we know the channel long profile associated with deposition of the terrace fill units. In any case, the valley long profile would seem to provide a better basis for comparison because it represents a long-term integrated record of the gradient of the fluvial system. In contrast, the channel long profile is subject to short-term change due to local variations in channel sinuosity.

The modern valley gradient remains relatively constant, at ~0.003, through the lower 12 km of the Clearwater-Queets drainage and across the inner continental shelf. The gradient increases at ~12 km offshore and becomes very steep beyond 25 km, which marks the head of a submarine canyon incised into the shelf edge. The shelf is typically ~40 km wide elsewhere but only 25 km wide offshore of the Queets-Clearwater drainages because of the headward incision of the submarine canyon.

Consider now what would happen during falling sealevel. During the early part of the fall, the river would extend its channel outward across the continental shelf. This extension would require little or no change to the upstream part of the drainage, given the similar gradient of the lower part of the river and the inner shelf. However, when sealevel dropped below about −50 m amsl, the Queets-Clearwater River would start to drain through the head of the Queets submarine canyon. The steeper gradient of the river in the canyon head would initiate a landward-migrating knickpoint. The knickpoint never made it to the mouth of the Queets, given that there has been no significant bedrock incision at the mouth of the Queets. From this, we conclude that the shelf has served to isolate the Queets-Clearwater drainage from the effects of eustasy. Apparently, the lowstands were not of sufficient duration to allow the knickpoints to reach the coast. An increased sediment flux may have driven aggradation

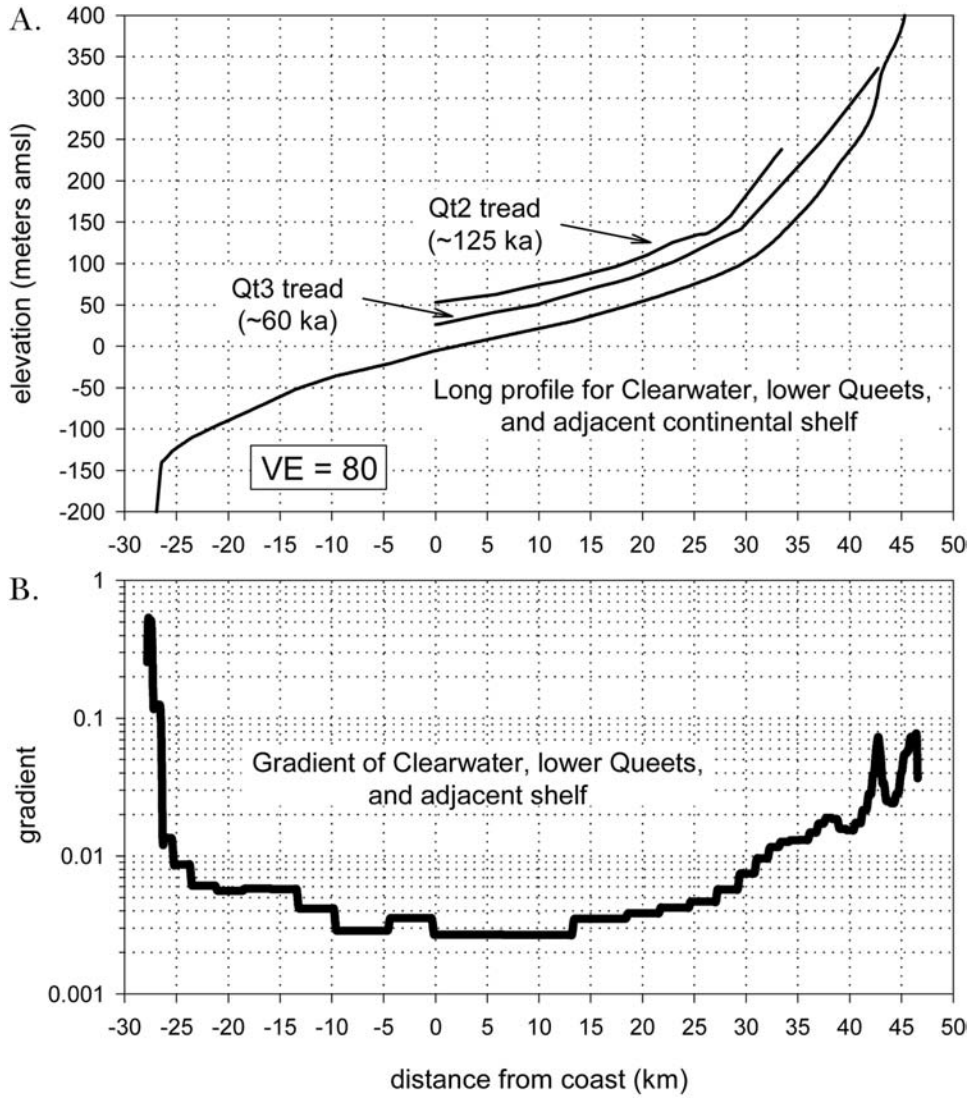

Fig. 12 (A) Relationship of the Clearwater and lower Queets rivers to the adjacent continental shelf. The valley long profile is used for the Clearwater and lower Queets. The shelf profile extends from the mouth of the Queets, orthogonal to the coast and ends at the head of the Queets submarine canyon. For comparison, we show the projection of the Qt2 and Qt3 treads into the valley profile (taken from fig. 7). (B) Gradient of the valley and shelf along the Clearwater and lower Queets. Note that the gradient remains approximately constant for ~12 km either side of the coastline.

during times of low sealevel, but our onshore evidence indicates that times of high sediment flux are roughly correlated with times of rising sealevel.

We propose that deposition of the thick Qt2 and Qt3 terrace fills occurred during rising sealevel and were driven by an enhanced sediment discharge associated with alpine deglaciation. This proposal seems the only solution capable of explaining the considerable height of the terrace treads at the modern coast: ~60 m amsl for Qt2 and ~30 m amsl for Qt3. Rates of tectonic uplift at the coast (specific estimates are given below) are much too slow to account for these high terrace treads. In fact, we can see

that the Sangamon wave-cut surface still lies close to the original height at which it was cut.

Our argument to explain these observations focuses on the location of the coastline during deposition of Qt2 and Qt3. Figure 13 shows the original configuration of the Qt2a and Qt3a terrace treads restored for uplift landward of the coast (see caption for details). During deposition, the actively aggrading surfaces of Qt2 and Qt3 would have had profiles that graded to a delta front. The delta front must have been inboard of the shelf edge and the top of the delta would have been close to contemporaneous sealevel. The gradient of the terrace treads across the shelf was probably similar to those portions still preserved near the mouth of the Queets (0.0005 and 0.0016 for the Qt2 and Qt3 treads, respectively).

These constraints were used to extrapolate the Qt2a and Qt3a treads across the continental shelf (fig. 13). This reconstruction shows that final deposition of Qt2a and Qt3a had to coincide with highstands. In correlating these units to specific highstands, we are guided by the fact that the units themselves were being fed by an increased sediment flux associated with deglaciation. Thus, we seek highstands at the end of glacial epochs. Given these constraints, we infer that deposition of Qt2a occurred at about 140 to 125 ka, while sealevel was rising to the Sangamon highstand. An extreme highstand of ~+5 m amsl is needed to accommodate the +60 m height of Qt2a at the

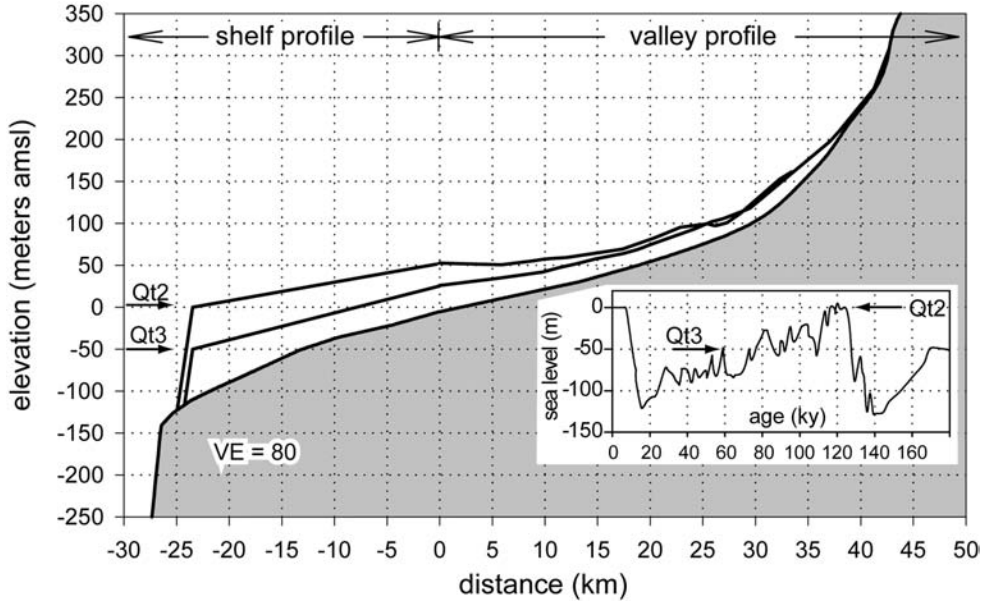

Fig. 13. Reconstruction of the initial configuration of the Qt2 and Qt3 treads. The following assumptions were used to extend the treads to the shelf edge: (1) the offshore continuation of the terrace tread should have had a gradient similar to the reconstructed gradient of the tread at the coast; (2) the terrace tread should have graded to contemporaneous sealevel; and (3) terrace deposition was not able to prograde beyond the shelf edge. These guidelines indicate that the terrace treads probably extended to close to the shelf edge, where they would have intersected delta fronts. We can estimate the ages of the terrace treads by comparing the elevation of that intersection (as marked by the arrows) with the eustatic sealevel curve shown in the inset (curve from Chappell and others, 1996). The Qt2a tread is correlated to the +5 m highstand at 122 ka (Sangamon), and the Qt3a tread is correlated to a -50 m highstand at 60 ka. Note that for completeness sake, we have restored the onland parts of the terrace treads for the effects of tectonic uplift. To do this, we took the profile of the treads in figure 12A and then lowered each point of the tread by an amount equal to the age of the tread multiplied by the local uplift rate. Uplift rates were taken from the smooth incision/erosion rate profile in figure 19.

coast. Deposition of Qt3a is attributed to a sealevel rise at 65 to 60 ka and would coincide with deglaciation associated with the end of IS4. The highstand at that time reached –50 m amsl, which gives a reasonable graded profile relative to the +30 m amsl height of the Qt3a tread at the coast.

These observations support the following synthesis of the Clearwater terrace stratigraphy (figs. 5 and 14). The oldest deposits are Qt1 and Qrd, as indicated by their high position in the landscape, deep weathering, and high degree of reworking. Rind-thickness measurements (figs. 9 and 10) suggest a middle Pleistocene age.

Qt2 was formed due to enhanced sediment supply liberated during the retreat of the Whale Creek alpine glaciers in the Hoh and Queets valleys. Rising sealevel allowed the unit to aggrade across the shelf to a coastline located close to the shelf edge. The abandonment of Qt2a marks a decrease in sediment supply. The geometry of the terrace tread suggests that abandonment occurred close to the time of the Sangamon highstand. From this, we infer that Qt2 was deposited at about 140 to 125 ka. When it was abandoned, one could look west from the present coast across a broad braided alluvial plain. The expanse of this plain is recorded by a seaward-thickening loess deposit on top of Qt2a, which was apparently derived from the area of the modern shelf by wind erosion associated with prevailing westerly winds.

Without the enhanced sediment supply to sustain it, Qt2 was quickly eroded back. The Clearwater-Queets river cut down through the deposit in an unsteady fashion, leaving behind a series of small cut-and-fill deposits (Qt2b-d). The shelf part of Qt2 was removed by wave erosion, which drove rapid retreat of a sea cliff, much like what is observed along the Olympic coast today. The retreating sea cliff left behind the wave-cut unconformity in its wake. The height of this unconformity at the coast indicates that it was cut during the Sangamon highstand at ~122 ka.

Qt3 is envisioned to have formed in similar way to Qt2. Lyman Rapids alpine glaciers are thought to have retreated in association with global warming and rising sealevel at the end of IS 4. Again, flushing of glacial debris provided an increased sediment flux through the Snahapish divide and into the lower Clearwater and Queets valleys. The increased sediment flux accounts for the aggradation. Our best guess is that Qt3 was deposited at ~65 to 60 ka during the transition from IS 4 to 3, when sealevel reached a local highstand of ~ –50 m amsl.

Qt4 is in some ways analogous to Qt2 and Qt3 in that it was deposited during the transition from the glacial IS 2 to the interglacial IS 1 (Holocene). What is different is that Qt4 is much smaller in extent and volume relative to Qt2 and Qt3. The reason is that alpine glaciation during the last glacial maximum was much smaller in extent relative to previous glacial epochs (Thackray, 2001). This point is illustrated by figure 4A, which shows the more limited extent of the Hoh Oxbow and Twin Creek moraines relative to the older Lyman Rapids and Whale Creek moraines (fig. 4A). Thackray (2001) argues that a drier climate during the last glacial maximum resulted in smaller alpine glaciations. Stratigraphic relations indicate that there was no spillover of outwash sediment from the Hoh into the lower Clearwater during Qt4 time. Thus, Qt4 aggradation was "sediment starved" and could not prograde outward like Qt2 and Qt3. This result illustrates that for the Clearwater-Queets system, progradation across the shelf only occurs when both sediment flux and sealevel are high.

The Holocene has been mainly a time of major valley incision and the carving of straths, although the straths are much narrower than their Pleistocene counterparts. The Qt5 and Qt6 terrace units are relatively thin and probably have little preservation potential. Wegmann and Pazzaglia (submitted) propose that deposition of these units was controlled by short-term climate change and earthquake-induced mass wasting from hillslopes.

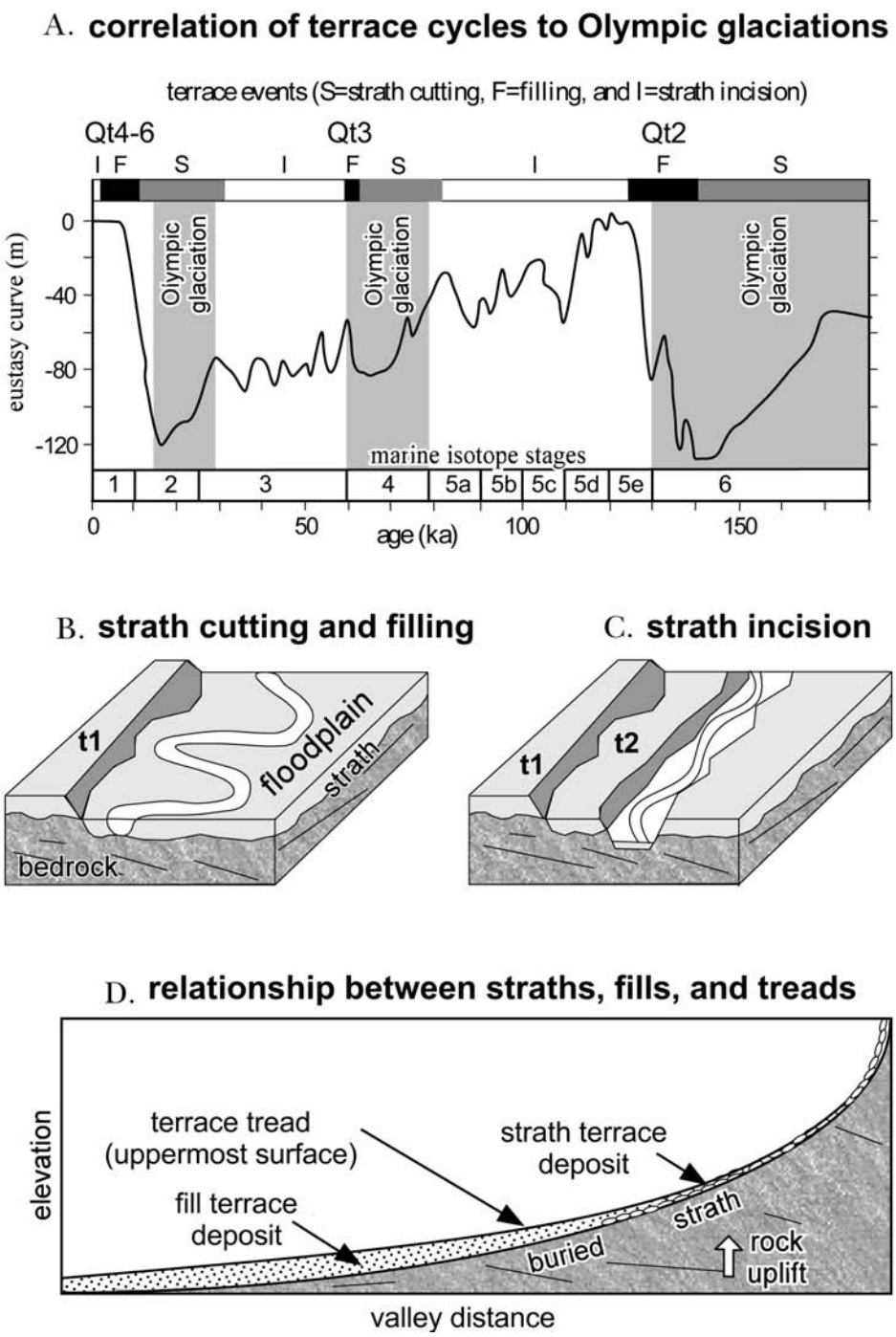

Fig. 14. Interpretation of the formation and timing of terrace cycles in the Clearwater drainage. (A) Terrace cycles appear to be linked to the global climate cycle, which is represented here using the marine oxygen isotope curve (after Fuller and others, 1998). Light-shaded regions indicate global glacial climates, which prevailed during IS 2-3, 4, and 6. (B and C) Illustration of a terrace cycle, which starts with cutting of a strath during a period of wide incision, followed by burial of the valley floor during an aggradational event, and ending with narrow incision through the fill and underlying strath. A complete cycle leaves behind a terrace unit (for example, t1 and t2). (D) Illustration of age relationships for straths and treads. Straths may be formed over a long period of time, but the form of the strath, as preserved in the stratigraphic record, dates to when the strath was buried. The deposition of a fill sequence in the lower reach of a river generally causes the entire river channel to aggrade. The implication is that the strath surface was probably abandoned at the same time along the entire channel. In contrast, fill deposition can vary considerably along the length of the river. The general tendency is that aggradation will persist for a longer time in the downstream reach, with the result that terrace treads generally young in a downstream direction.

Age of straths.—Having estimated the age of the terrace units and their treads, we now consider the age of the underlying straths. We focus here on the Qt2 and Qt3 straths, which are used below to estimate incision rates. Evidence cited above indicates that Qt2 and Qt3 deposition started toward the end of a glacial epoch. From this we infer that the straths were cut sometime during the glacial part of the climate cycle ("S" in fig. 14A). However, for our analysis of incision rates, we need to estimate when the straths were buried, not when they were formed. Burial ages are estimated using the older limits for the ages of the overlying fill: 140±20 ka for burial of the Qt2 strath and 65±10 ka for the burial of the Qt3 strath. These estimates are crude, as indicated by the cited uncertainties. Nonetheless, the age uncertainties are small relative to the absolute ages of the straths and the difference in their ages. Qt2a and Qt3a appear to have been deposited within a short period time (5 - 15 ky), coincident with rising sealevel. Thus, burial of the straths probably occurred rapidly along the entire length of the valley. As a result, we are confident that the Qt2 and Qt3 straths provide good "snapshots" of the long profile of the valley floor.

INCISION OF THE QT2 AND QT3 STRATHS

Our estimates of fluvial incision are based on the height above the modern channel of the Qt2 and Qt3 straths, which are the widest and most continuous straths in the Clearwater drainage. By definition, these straths were cut when the river was carving out a predominantly bedrock-floored valley bottom. The modern river is also carving out a bedrock-floored valley bottom. Thus, we suggest that the modern valley profile of the Clearwater is a close approximation for the valley profile during the cutting of the Qt2 and Qt3 straths. If correct, then fluvial incision would be equal to rock uplift. We test this possibility below. For now, we focus on the amount, pattern, and rates of fluvial incision. Note that by measuring straths height, we are purposely ignoring the incision of the river through any overlying fill. The reason is that rock uplift is equal to the amount of bedrock incision, not total incision, assuming, of course, that our assumption above holds, that the river valley returns to the same long profile during each phase of strath formation.

Bedrock incision was measured using two methods. The strath height above the channel was measured using an altimeter to obtain relative vertical elevation, which has a cited two standard error (2SE) precision of 1 m. Some straths greater than ~20 m above the modern channel were measured by positioning the modern channel and the strath relative to the 12 m contours on United States Geological Survey 7.5 min topographic maps. We use a relative standard error (RSE) of 5.5 percent to represent the uncertainty for all height measurements.

Estimated incision rates are affected by errors in both height and age. The approximate uncertainties (~2SE) for the age of strath burial are: Qt2 = 140 ka ± 20 ky (±14 percent) and Qt3 = 65 ka ± 10 k.y. (±15 percent).

Incision measurements for the Qt2 and Qt3 straths are shown in figure 15A and B. Incision rates are presented in figure 15C. The error bars for the incision rates include only height errors because the uncertainty in strath age is common to all incision rates from the same strath. The uncertainties for both height and age give a combined uncertainty of 2RSE ~ 18 percent.

Both Qt2 and Qt3 straths show increased incision in the upstream direction. Incision rates are remarkable similar for both straths (fig. 15C). Smooth curves fit to the data indicate incision rates ranging from ~0.0 m/ky at the coast to ~0.9 m/ky in the upper Clearwater valley (fig. 15). The plots also show locally fast incision between km 15 and 20 (fig. 15). This feature is coincident with the convexity in the valley long profile described in figure 5. The downstream portion of that convexity has the highest sinuosity of the entire Clearwater channel, whereas the upstream portion has relatively

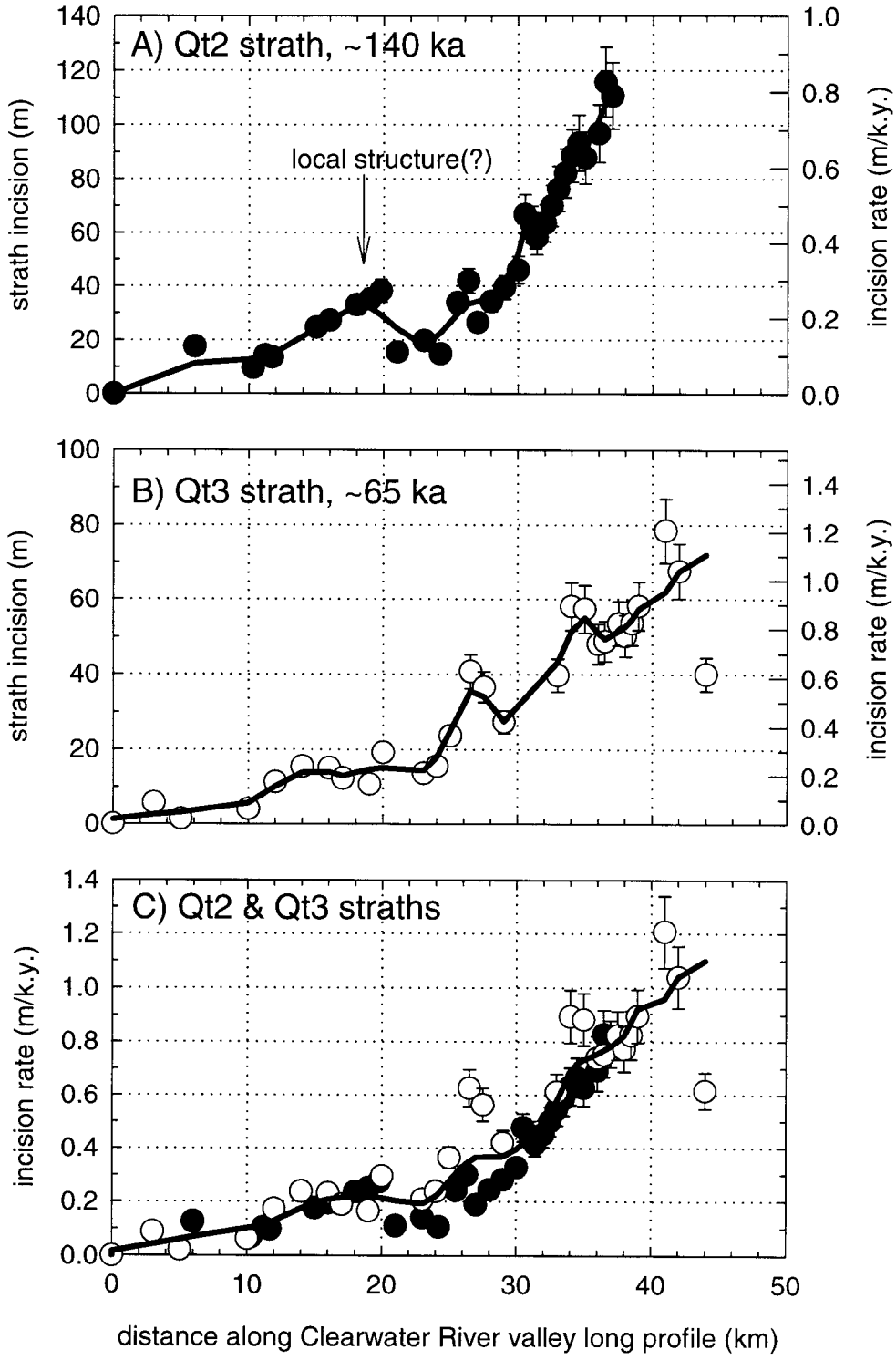

Fig. 15. Incision of the (A) Qt2 and (B) Qt3 straths with respect to distance along the valley long profile (see fig. 4B). (C) Incision rates calculated from the Qt2 strath (solid circle) and Qt3 strath (open circle). Note the similarity in the estimated long-term incision rates for these two different-age straths. In general, incision and incision rates increase in an upstream direction. The small bump in the profiles at about 15 to 25 km suggests some localized uplift, such as a broad fold. Error bars show ±2SE uncertainties due to measurement errors for strath height. The thick lines are smoothed from the original data using a locally weighted regression method (Lowess algorithm of Cleveland, 1979, 1981, with the interval parameter set to 0.2).

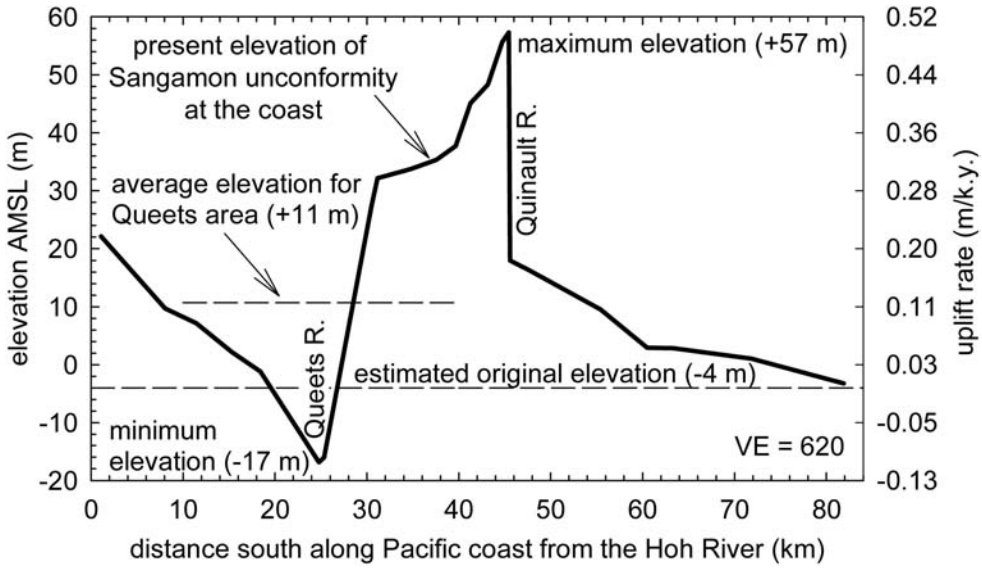

Fig. 16. Section showing the elevation of the Sangamon unconformity (122 ka) as exposed along the west coast of the Olympic Peninsula (from McCrory, 1996). The lower dashed line at −4m amsl shows the elevation that the exposed unconformity was formed at. The upper dashed line shows the ±17.5 km window used for the long-term erosion-rate data shown in section A-A′ of figure 19. The unconformity has an average elevation within that window of +11 m, indicating an average uplift rate of 0.12 m/ky section A-A′ crosses the coast.

low sinuosity (inset map in fig. 5). The convexity is apparent only on the valley long profile and not on the channel long profile (fig. 5). These adjustments in channel sinuosity are consistent with the predicted tectonically-driven changes in the valley gradient (Ouchi, 1985; Schumm, Dumont, and Holbrook, 2000). Similar behavior is observed where alluvial rivers cross actively growing folds. The long-term integrated deformation associated with the localized uplift is well expressed in the deformation of the Qt2 and Qt3 straths (fig. 15A and B). This structure is probably similar to other local structures, mainly broad folds, known to deform Quaternary deposits in the western Olympic Peninsula (McCrory, 1996; Thackray, 1998).

UPLIFT ALONG THE COAST

Strath incision provides some information about uplift rates at the coast, but that record is limited to the mouth of the Queets River. The Sangamon unconformity provides a more extensive datum for measuring uplift along the coast. McCrory (1996) and Thackray (1998) published detailed profiles of the unconformity, as exposed for ~80 km, adjacent to the mouth of the Queets River (fig. 16). The unconformity is gently warped into long wavelength folds (fig. 16) with horizontal northeast-trending axes. The height of the unconformity ranges from -17 to +57 m, with an average of +18 m.

To estimate uplift, we need to know the water depth at which the exposed parts of the unconformity formed. Uncertainties here are cited at ±1 SE. The coastal exposures of the unconformity lie seaward of a Sangamon sea cliff (figs. 11 and 17). This fossil cliff marks the farthest landward advance of the coastline during the 122 ka highstand. The cliff is presently partially buried beneath the "30 m" terrace unit (= Qt3). In general, the Sangamon sea cliff lies about 1450 ± 50 m inland of the modern sea cliff, which in turn lies about 50 m inland from the modern shoreline. This

Fig. 17

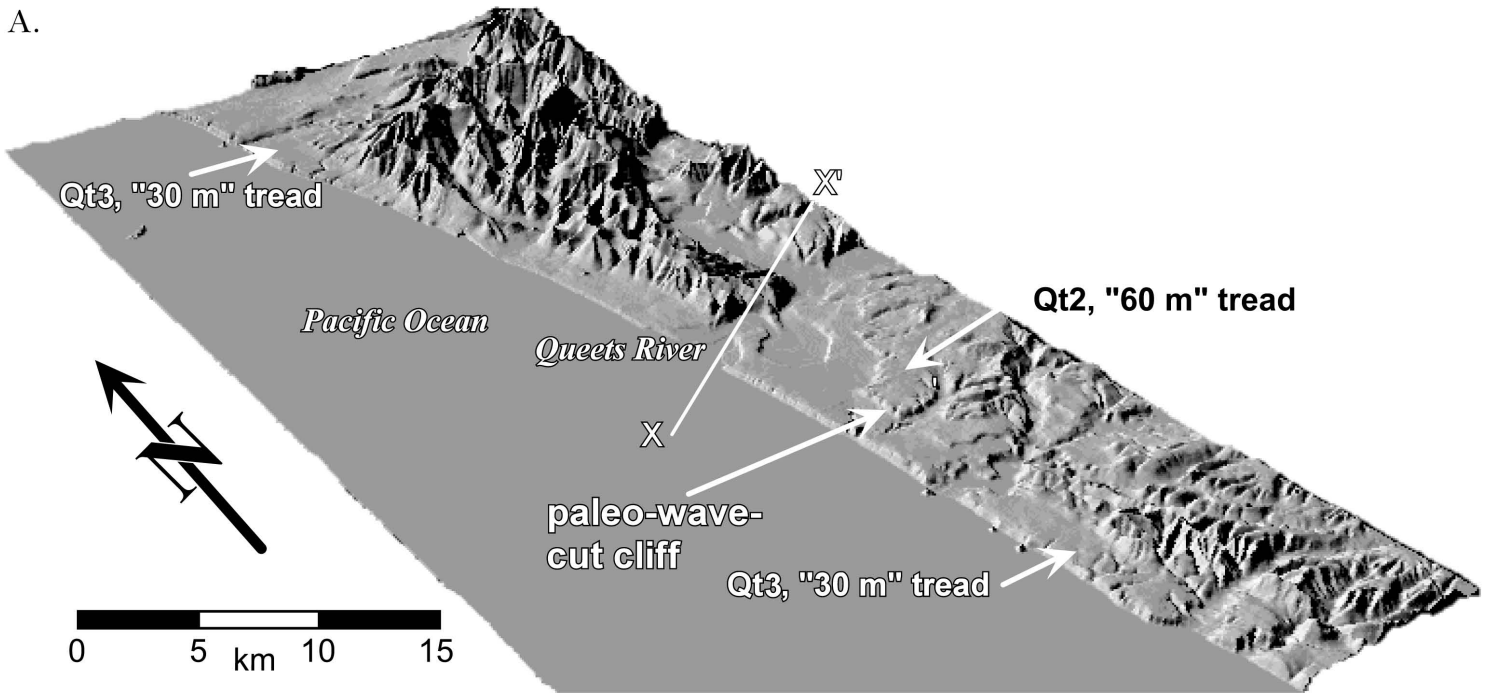

(A) Digital shaded relief showing the buried Sangamon sea cliff. The cliff shows up as subdued scarp, which parallels the coast at a distance 1500 m inland from the coast. The feature is visible in the image from ~15 km south to ~5 km north of the Queets River.

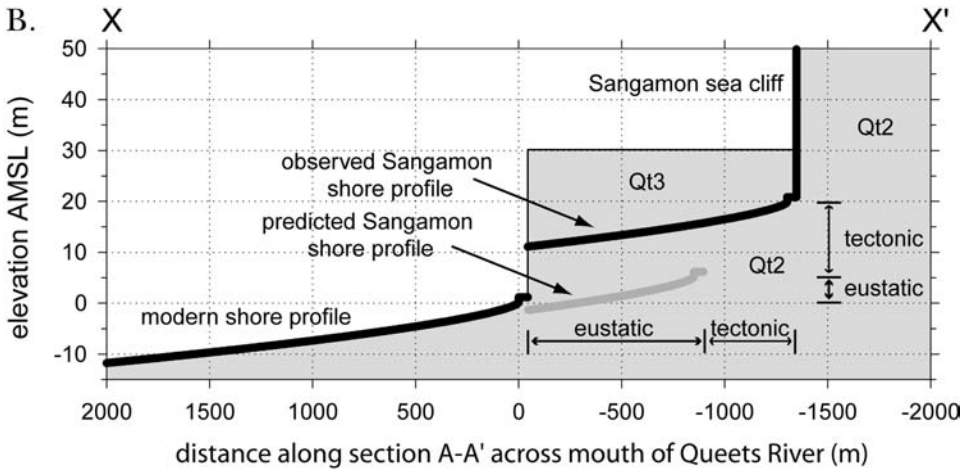

(B) A schematic cross section of the modern shoreface and sea cliff and the buried Sangamon sea cliff at the mouth of the Queets River. The section X-X′ follows A-A′; it has an azimuth of 54°, parallel to the plate convergence direction.

relationship is consistent from 15 km south to 5 km north of the Queets River (fig. 17A).

The present shoreface profile is used as a proxy for the Sangamon shoreface since both were cut into loose fill of the coastal terrace sequence. Bathymetric contours are relatively smooth and trend parallel to the coast, even near the mouth of the Queets. Bathymetry from the USGS Queets 7.5 minute map was fit using a standard shoreface function, $z = A\,x^{2/3}$ (p. 6 in Trenhaile, 1997), where x is the offshore distance, z is the depth below mean sealevel, and A is a fit parameter. The shoreface function fits the data well, with $A = 0.0698 \pm 0.0022$. At 1450 ± 50 m offshore of the present coast, the seafloor is at -9.0 ± 0.35 m amsl. Because the Sangamon highstand is estimated to have been $+5 \pm 0.7$ m amsl (the ± 2 m uncertainty cited by Chappell and others, 1996, is taken as ± 3 SE), we infer that exposures of the Sangamon unconformity along the modern coast adjacent to the Queets would have originally formed at an elevation of -4.0 ± 0.8 m amsl.

This initial water depth, together with the age of the unconformity, allows estimates of rock uplift rates (see right axis of fig. 16). The mouth of the Queets is subsiding at ~0.1 m/ky. This low rate is consistent with the convergence of strath surfaces toward the mouth of the Clearwater (figs. 7 and 15). But what about the broader area around the Queets? To answer this question, we consider all the data within a ±15 km window parallel to the coast (see upper dashed line in fig. 16). (Note that this window is the projected dimension of a ±17.5 km wide window used below in our discussion of uplift and erosion rates along section A-A′.) The average elevation of the unconformity in the window is +11 m amsl, which indicates an uplift of +15 m and an average uplift rate of ~0.12 m/ky where section A-A' crosses the coast.

More rapid uplift is observed ~20 km south of the Queets River (fig. 16). There, the north side of the Quinault River is rising at a rate of 0.50 m/ky. One interpretation is that this fast uplift is localized above a rising fold, associated with the north-south shortening recognized by McCrory (1996) and Thackray (1998). Another possibility is that the uplift is related to local intrusion of mud diapirs, which are common in that area (Rau and Grocock, 1974; Orange, 1990).

Horizontal displacement of the Sangamon sea cliff.—In general, rocks at the earth's surface move in both vertical and horizontal directions (Willett, Slingerland, and Hovius, 2001). The Qt2 and Qt3 straths and the Sangamon wave-cut bench give no information about the horizontal component of motion. However, the Sangamon sea cliff does provide information about horizontal displacements relative to the coast. Based on the apparent rapid retreat of the coastline during Sangamon time (as discussed above), it would seem that a retreating sea cliff is able to adjust rapidly to rising sealevel. Thus, we assume that the horizontal distance between the Sangamon and the modern sea cliff is due solely to eustasy and tectonic displacement.

We used Bruun's rule (Dean, 1991) to estimate how much the modern sea cliff would be translated landward if modern sealevel were to rise to the height of the Sangamon highstand. According to this relationship, a rise in sealevel S would cause a landward shift in the shoreline of

$$\Delta x = S w_w/(h_w + h_b), \tag{1}$$

where w_w and h_w are the width and maximum depth of the breaker zone, and h_b is the berm height on the beach. A 17 yr record for a deep-water (2780 m) buoy offshore of the Queets River indicates that waves coming into that coastline have maximum heights of 13.6 m and maximum periods of 18 seconds in the open ocean (buoy 46005, National Data Buoy Center, 2000). Using relationships in Trenhaile (1997, p. 22), these waves indicate a maximum breaker depth $h_w = 14.0 \pm 1.0$ m (uncertainties are once again $\pm$ 1 SE). The nearshore profile indicates that this depth lies offshore at $w_w = 2850 \pm 220$ m. The berm height h_b is ~1 m. Bruun's rule indicates that if modern sealevel were to rise to the Sangamon highstand ($S = +5 \pm 0.7$ m), the Sangamon sea cliff should have formed 945 ± 145 m inland with respect to the modern sea cliff. The sea cliff presently lies 505 ± 150 m farther inland, a difference we attribute to tectonic displacement.

Tectonic displacement of the sea cliff line is assumed to have occurred parallel to the convergence direction (A-A′), which is 26 degrees counterclockwise from the normal to the coast line. The cross section in figure 17B was constructed along A-A′ at the mouth of the Queets and shows both the horizontal and vertical components of the displacement, along with the predicted eustatic and tectonic components of those displacements. The predicted horizontal tectonic displacement is 450 ± 135 m, accomplished over 122 ± 2 ka, which gives a long-term horizontal tectonic velocity of 3.7 ± 1.1 m/ky relative to the adjusted highstand shoreline.

Our interpretation of this result relies on the assumption that the Olympics are in a long-term steady state, meaning that the range is not changing in size with time. This steady-state configuration implies that the shoreline is also in steady state. More specifically, we are assuming that the shoreline returns to the same location at each highstand. Of course, in practice, one would have to correct for small differences in the height of successive highstands (as we have done above). The overall implication is that when the shoreline is at steady state, erosion in the breaker zone is balanced by uplift at the coast. In this case, the calculated tectonic displacement of the Sangamon sea cliff would represent the horizontal velocity of rocks at the coast relative to the long-term steady-state position of the shoreline. An alternative interpretation is that the Olympics are not in steady state, and the shoreline is moving westward as the mountain range increases in size and width. The coastal geomorphology does not provide any information to distinguish between these two end-member interpretations. However, we do show below that frontal accretion into a steady-state Olympics wedge would produce horizontal surface velocities at the coast of 3 m/ky. Thus, the sea cliff observations are consistent with a steady-state wedge interpretation.

DISCUSSION

The Qt2 and Qt3 straths show that long-term incision rates in the Clearwater drainage increase from <0.1 m/ky at the coast to ~0.9 m/ky in the upper part of the drainage. Furthermore, the fossil Sangamon sea cliff indicates that rocks at the mouth of the Queets may be moving to the northeast at ~3.7 m/ky relative to the long-term position of the highstand shoreline. In this section, we consider how these geomorphic measures might relate to actual rock velocities. We examine three specific issues. The first is the relationship between strath height and fluvial incision. The two are commonly thought to be equal, but this is not the case when horizontal displacements become significant. The second issue concerns the long-held assumption that that a river valley returns to the same long profile during each phase of strath formation. If correct, then vertical incision rates should be equal to rock uplift rates. Finally, we use a simple kinematic model to consider how surface velocities, as estimated from our geomorphic measurements, relate to regional-scale accretion and deformation of the Cascadia wedge.

Strath separation.—Fluvial incision is usually defined to mean the amount of vertical incision of the river channel. An implicit assumption is that an incised strath has risen vertically from the river channel, but there is evidence that the bedrock around the Clearwater may be moving both upward and horizontally to the northeast relative to the Clearwater River. Thus, what we have really measured is *strath separation,* which is the vertical height of the strath above the modern channel, without any reference to the original point of formation in the ancient river channel.

Consider the problem as illustrated in figure 18A. The river channel is taken to be at steady state, with the rate of vertical incision equal to the rate of rock uplift. The vectors show rock velocities at the surface with u and w indicating the horizontal and vertical components of the velocity vector. The velocity field is assumed to be two-dimensional and to lie within the x-z plane. The rate of strath separation is given by

$$w' = w - gu \tag{2}$$

where g is the gradient of the river channel after projection into the x-z plane. The gradient is measured in that plane because the points of the strath are, by definition, moving in that plane.

Figure 18B illustrates the relationship between w' and w for the case of full frontal accretion in the Olympics. The surface velocity field is based on a kinematic model presented below. For now, it is sufficient to say that frontal accretion tends to produce the largest horizontal velocities within an accreting wedge, so that the difference between w' and w will be maximized for this situation. For the Clearwater, the velocity field is inferred to parallel section A-A′, so g is determined by projecting the river channel into A-A′ (fig. 18B). There is little difference between w and w' until km 30 where the g gets large. Even in this part of the profile, the difference between w and w' is <10 percent. Thus, in the Clearwater, it seems reasonable to equate w' with w. This conclusion is not universal. For instance, large differences between w' and w should be expected in areas where g is large or $u > w$. Willett, Slingerland, and Hovius (2001) provide a general discussion of this topic in their treatment of advection of topography in horizontally shortening mountain ranges.

Test of the steady-state assumption.—We show above that the Qt2 and Qt3 straths record similar incision rates (fig. 15). This observation has several important implications: (1) during strath formation, the valley profile appears to be able to quickly reach and maintain a steady-state form; (2) bedrock incision appears to be balanced over the long term with rates of rock uplift; and (3) tectonic forcing appears to be steady over the long term as well. These conclusions are interesting given that the river system itself is relatively unsteady. For example, the terrace sequences record cyclic alternation

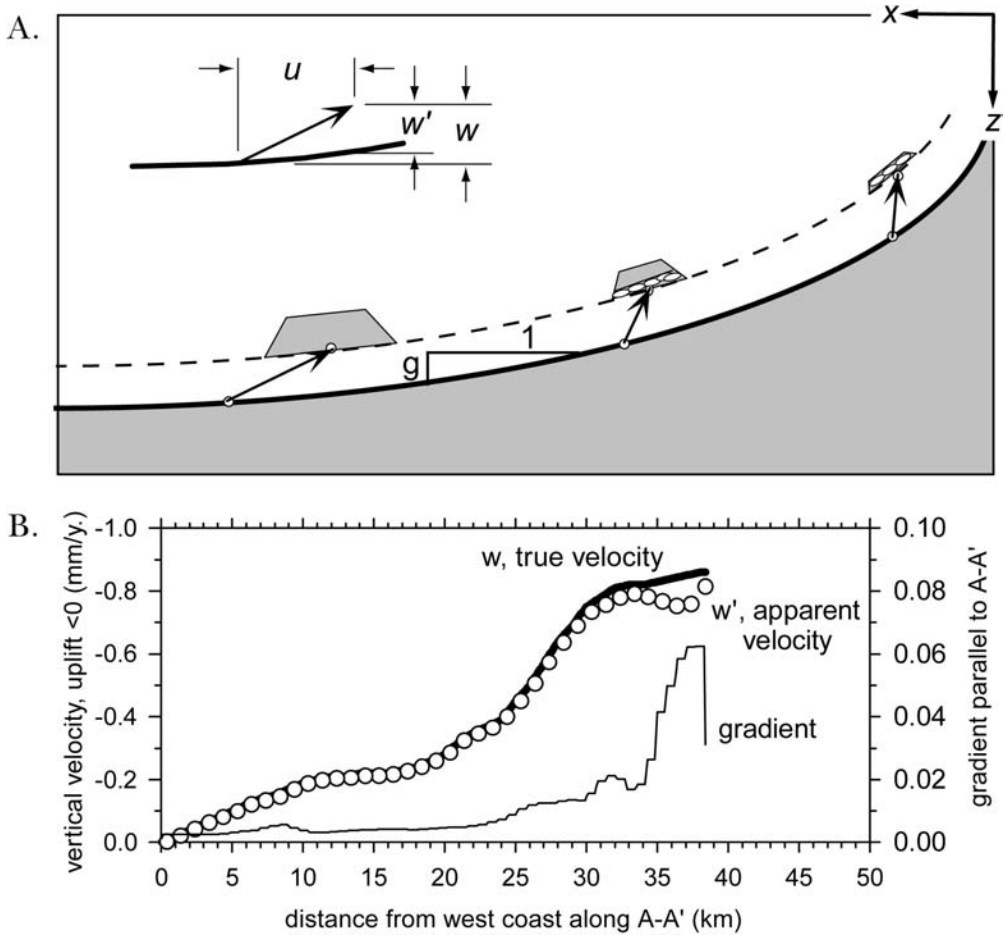

Fig. 18(A) Illustration of how the horizontal and vertical components of the rock velocity vector, u and w respectively, control w', the rate of separation of the strath from the river channel. The section is oriented parallel to the rock velocity vector and is defined by coordinate directions x and z. The variable g is the gradient of the channel after projection into the x-z section. (B) Example for the Olympics using the observed g and estimates for u and w calculated from a kinematic model assuming full frontal accretion (discussed below, see figure 20A for broad details). Full frontal accretion produces the largest horizontal velocities and should maximize the difference between w and w'. The rock velocity vector is assumed to have a trend parallel to the modern plate convergence direction. The gradient g is measured using the channel as projected into section A-A'. For the Olympics, there appears to be little difference between w and w', even when horizontal velocities are large.

between incision and aggradation. The steadiness only shows up when we look at time scales longer than a terrace sequence. An analogous situation exists for subduction zones: slip on the subduction thrust occurs episodically during major earthquakes, but the convergent motion of the plates is steady when averaged over several earthquake cycles.

Here we examine other evidence for long-term steady state that extends beyond the immediate long profile of the Clearwater River. If our interpretation for a steady-state orogen is correct, then we should see a close correspondence between erosion rates and incision rates. Section A-A′ in figure 19 shows a comparison of strath incision rates for Qt2 and Qt3 with long-term erosion rates estimated from apatite

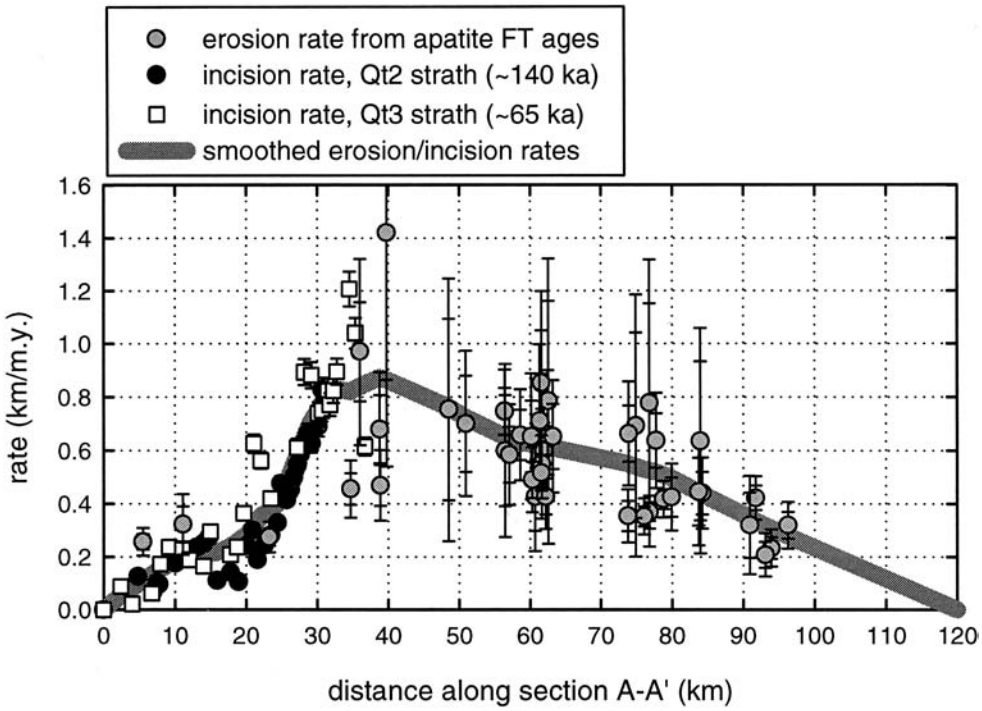

Fig. 19. Comparison of short-term fluvial incision rates with long-term erosion rates, as estimated from reset apatite fission-track ages. The similarity of these rates indicates that the Olympics uplift is in a flux steady state. Fission-track-based erosion rates were selected from a ±17.5-km wide window centered on section A-A′. Error bars show ±1SE uncertainties; error bars for incision rates only accounts for errors in height measurements (as discussed in text). The thick gray line shows a smoothed curve for the rate data, as estimated using a locally weighted regression method (Lowess algorithm of Cleveland, 1979, 1981, with the interval parameter set to 0.2). Reset apatite fission-track ages are from Brandon, Roden-Tice, and Garver (1998) and Brandon and Roden-Tice (unpublished data). Long-term erosion rates were estimated using the method in the appendix of Brandon, Roden-Tice, and Garver (1998).

fission-track ages (see Brandon, Roden-Tice, and Garver, 1998, and Batt and others, in press, for details). There is good agreement between these two very different data sets, right down to the localized uplift recognized at km 18 along the valley long profile (see figs. 6 and 15). Note that the strath data integrate incision rates over a ~100 ky time scale, whereas the fission-track ages integrate over a ~7 my time scale. The similarity of incision and erosion rates over these very different time scales supports the interpretation that, on the long-term, the valley profile of the Clearwater has been a steady-state feature of the landscape.

The heavy gray line represents a smoothed version of the erosion-rate/incision-rate profile along A-A′ across the Olympics. This profile provides information about the total erosional flux across the Olympics uplift. Brandon, Roden-Tice, and Garver (1998) argue that there is a close agreement between the accretionary influx and erosional outflux for the Olympics wedge. The smoothed rate profile in figure 19 indicates an erosional flux of 51 km^2/my, which is close to the estimated modern accretionary flux, ~63 km^2/my (Brandon, Roden-Tice, and Garver, 1998). Batt and others (in press) provide a more rigorous test of the flux steady-state interpretation by using a full two-dimensional kinematic-thermal calculation to model the thermochronologic and incision-rate data. Best-fit solutions indicate that the data are fit well by predictions of a steady-state model.

Velocity field beneath the Cascadia forearc high.—If the wedge maintains a long-term steady-state balance between accretionary and erosional fluxes, then the wedge will not grow in size. The steady flux through the wedge allows us to construct a simple kinematic model, which we use to illustrate possible velocity fields within the wedge. The details of the model are described in the appendix.

One feature of the model is that it can be used to examine the relative roles of underplating and frontal accretion. Examples of predicted velocity fields are given in figure 20. Figure 20A shows a case where all accretion occurs through the front of the wedge (frontal accretion), whereas figure 20B illustrates the case where accretion occurs solely at the base of the wedge (underplating). Figure 20C has an even mix of underplating and frontal accretion. Note that the uplift rate profile (w) is based on the smoothed incision-rate/erosion-rate curve estimated in figure 19. Thus, all the velocity fields have the same pattern of vertical velocity at the surface. Where they differ is in their horizontal velocities. The frontal accretion example has the largest horizontal velocities, whereas the underplating example has zero horizontal velocities.

An important implication is that erosion rates and terrace uplift rates do not provide any useful information about the horizontal velocities at the wedge surface. Our main source of information about horizontal velocities comes from the translated Sangamon sea cliff. In fact, the frontal accretion example predicts 3 m/ky at the coast, which compares well with the ~3.7 m/ky determined from the sea cliff. We take this match as evidence that the Olympic portion of the Cascadia wedge is dominated by frontal accretion. The modeling of Batt and others (in press) also indicates that the wedge is growing mainly by frontal accretion.

The velocity fields also show the distribution of deformation within the wedge. Note that the deformation shown in the model calculations is steady and permanent. Elastic distortions associated with the earthquake cycle would be superimposed on this steady deformation. Each example includes a plot of D_{xx}, the horizontal strain rate at the surface of the wedge. The horizontal velocity w and horizontal strain rate D_{xx} are greatest for pure frontal accretion and zero for pure underplating. Frontal accretion tends to cause larger horizontal strain rates toward the front of the wedge because the wedge is thinner there and because the horizontal flow within the wedge requires some vertical thickening to maintain the steady-state form of the wedge.

We can compare these model calculations with GPS measurements of horizontal velocities across the Olympics for benchmarks shown in figure 1B (Z. Ning and A. Qamar, written communication, 2001). The data in vector form had directions that were withn ±20° of the predicted convergence direction for Juan de Fuca relative to North America. GPS velocities shown in figure 21 have been projected into the A-A′ section and are calculated relative to a fixed point at 0 km along A-A′, which is the reference frame used for our kinematic model. The curve showing long-term horizontal velocities comes from the full frontal-accretion model illustrated in Figure 20A. This comparison indicates that long-term horizontal velocities across the Olympics may account for 20 to 35 percent of the geodetically measured horizontal velocities.

Savage, Lisowski, and Prescott (1991) report results from a local strain network operated in the eastern Olympics at ~30 km along section A-A′. The network indicates a maximum shortening direction in the horizontal at 59° ± 6.6° azimuth, which is approximately parallel to the estimated modern convergence direction at 54°. The strain rate in this direction is −0.092 ± 0.028 μstrain /yr. In comparison, the permanent strain predicted at 30 km for pure frontal accretion is −0.01 μstrain/yr. In this case, the permanent deformation accounts for only 10 percent of the geodetically measured deformation. Note that the strain network is from the eastern Olympics where both permanent and elastic deformations are probably relatively slow.

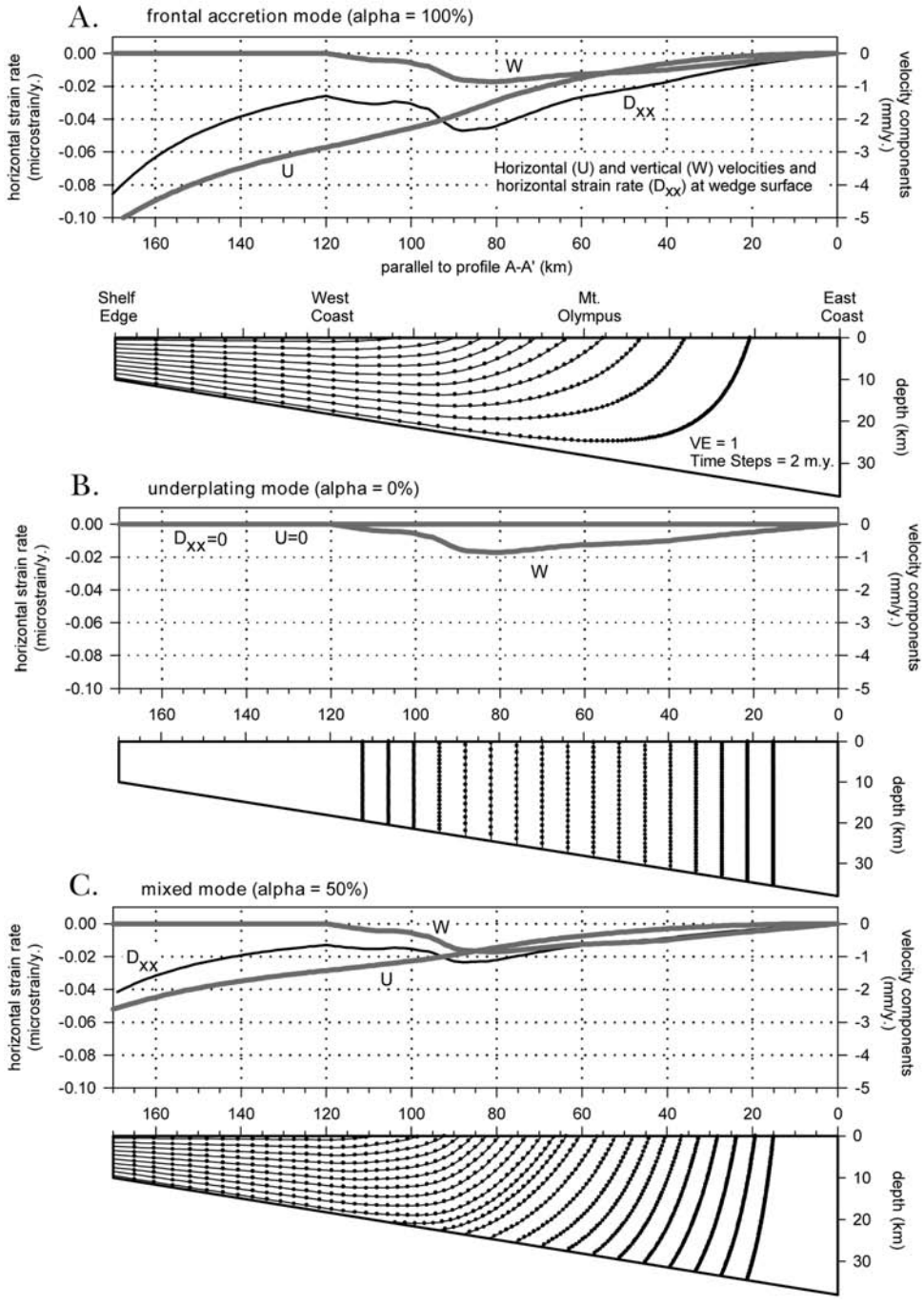

Fig. 20. Several solutions for flow fields in the Cascadia wedge across the Olympic Peninsula (section A-A'). The flow fields show the average velocity field and displacement paths at the scale of the entire wedge; local heterogeneities, caused by faulting and folding, are assumed to average out at this scale. The solutions are described in the text and the appendix. (A) The frontal accretion solution assumes that all accretion occurs at the front of the wedge. (B) The underplating solution assumes accretion entirely by vertical underplating at the back of the wedge. (C) The mixed solution assumes 50 percent frontal accretion and 50 percent underplating. The plots at the top of each cross section show the model estimates for horizontal strain rate D_{xx} and the horizontal u and vertical w velocities at the surface of the wedge. The northeast side of the wedge is held fixed. $D_{xx} < 0$ indicates horizontal shortening, and $u < 0$, a northeast velocity, and $w < 0$, upward velocity. The solutions assume a steady-state balance between the accretionary influx and the erosional outflux for the wedge. The vertical surface velocities w are set equal to the smoothed curve for long-term incision/erosion rates, as shown in figure 19.

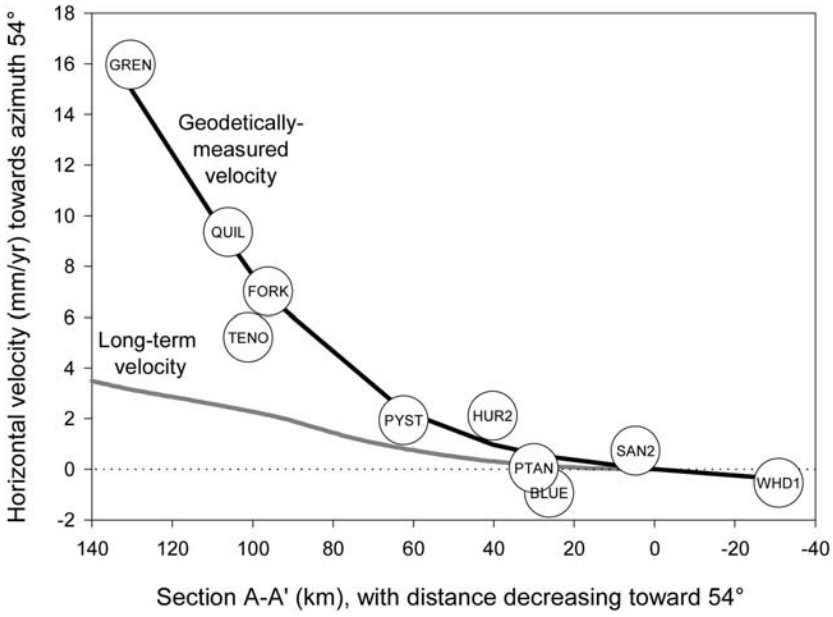

Fig. 21. Comparison of geodetically measured horizontal velocities and long-term horizontal velocities in section A-A′. Geodetic velocities are from GPS measurements collected and analyzed by Z. Ning and A. Qamar (written communication, 2001). Velocities have been projected into the section, which parallels the modern convergence direction, and are referenced to a fixed point at 0 km along the section (northeast coast of the peninsula). Benchmarks are shown in figure 1B. Long-term horizontal velocities are calculated from the kinematic model, assuming full frontal accretion (fig. 20A). The predicted long-term horizontal velocities account for 20 to 35 percent of the geodetically-measured horizontal velocities.

CONCLUDING REMARKS

Our study uses fluvial geomorphology to measure incision and rock uplift across the Olympics sector of the Cascadia subduction zone. A well-preserved terrace stratigraphy in an unglaciated drainage, together with reasonable age control for the terrace deposits, allows us to use the valley profile of the Clearwater as a crude geodetic datum. As such, we are able to look beyond the earthquake cycle, to quantify long-term patterns of deformation and uplift across the interior of the Olympic Peninsula, where sealevel is not available as a datum. We summarize 6 major conclusions here.

1. Fluvial terrace sequences in the Olympics appear to be closely tied to the glacial climate cycle, through its influence on local climate, sediment supply from adjacent alpine-glaciated drainages, and eustasy. The sequence of terrace-forming events is consistent with the model of Bull (1991), but the timing of these events relative to the eustatic cycle is quite different. Bull (1991) proposed that strath formation occurred during rising sealevel and aggradation during falling sealevel. In the Olympics, strath formation appears to occur during peak glaciation (when sealevel is low) and aggradation, during late glacial and interglacial times, when sealevel is rising. We suspect that this difference is a local effect, related to the strong influence that local deglaciation has had on sediment supply and the interaction of that enhanced sediment supply with rising sealevel during the transition to interglacial times.
2. The upstream divergence of straths in the Clearwater provides strong evidence that uplift is very slow at the coast and increases to a maximum in the center of the range. This conclusion runs counter to a commonly invoked assumption in

fluvial geomorphology that long-term uplift rates can be taken as uniform within a single drainage.

3. Straths of different ages show a similar pattern of incision rates along the Clearwater, ranges from < 0.1 m/ky at the coast to a maximum of 0.9 m/ky in the center of the Olympics. These rates correspond closely with the pattern of long-term erosion rates indicated by apatite fission-track cooling ages. These observations indicate that, at long time scales (> 10 - 100 ky), the average form of the landscape remains close to steady state. This also implies that that during each phase of strath cutting, the Clearwater valley profile is able to return to the same steady-state form. Thus, bedrock incision rates appear to be a reasonable proxy for rock uplift rates in the Olympics.
4. The profile of incision and erosion rates across the Olympics indicates a close balance between the accretionary and erosional fluxes moving in and out of the wedge. This result supports the hypothesis of Brandon, Roden-Tice, and Garver (1998) that the Olympics sector of the Cascadia wedge is close to a flux steady state, but note that this conclusion does not require the topography to be steady as well.
5. A buried sea cliff, probably formed at 122 ka, provides evidence of horizontal motion of rock relative to the modern shoreline. The rate of motion is 3.7 m/ky to the northeast, which is close to the 3 m/ky horizontal material velocity predicted for a frontally accreting steady-state wedge. If this interpretation is correct, then it implies that the shoreline takes on a steady state configuration with each highstand. As a result, we can view the northeast translation of the Sangamon sea cliff as recording northeast-directed shortening across the Olympics uplift.
6. Finally, we develop a simple kinematic model that allows us to use the erosion rate profile across the wedge to predict horizontal velocities at the surface of the wedge. This model shows that the largest horizontal velocities are associated with full frontal accretion. From this we show that long-term horizontal velocities may account for 20 to 35 percent of the geodetically measured horizontal velocities across the Olympics. Clearly, this conclusion has important implications for understanding seismic hazards associated with the Cascadia subduction zone.

ACKNOWLEDGMENTS

Pazzaglia acknowledges a post-doctoral position at Yale University and a faculty appointment at University of Mexico, which provided the opportunity and support for this research. Funds were provided by NSF Post-Doctoral Research Fellowships, EAR-9302661 and NSF EAR-9736748 to Pazzaglia and NSF EAR-8707442 to Brandon. Land access was kindly provided by the National Park Service, State of Washington, Rayonier Inc. Hoquium Division, and the Quinault Nation. Field assistance was provided by Karl Wegmann, Tony Garcia, Rebecca Bendick, John Garver, Mary Roden-Tice, Glenn Thackray, and Wendy Gerstel. Sean Willett is thanked for critical intellectual feedback that helped shape and sharpen many of our ideas and conclusions. Z. Ning and A. Qamar at University of Washington kindly provided preliminary GPS velocities. Harvey Kelsey and Brian Atwater reviewed an early manuscript, and Bill Bull, Kelin Whipple, and Peter Knuepfer provided formal reviews; we are grateful to all for their detailed comments and helpful criticism.

Appendix 1

We devise a simple steady-state kinematic model for the Olympics segment of the Cascadia wedge, which is used to compare various records of vertical and horizontal motions at the surface of the wedge. The model, which is shown in sketch form in figure A-1, is meant to represent the long-term average velocity field for the

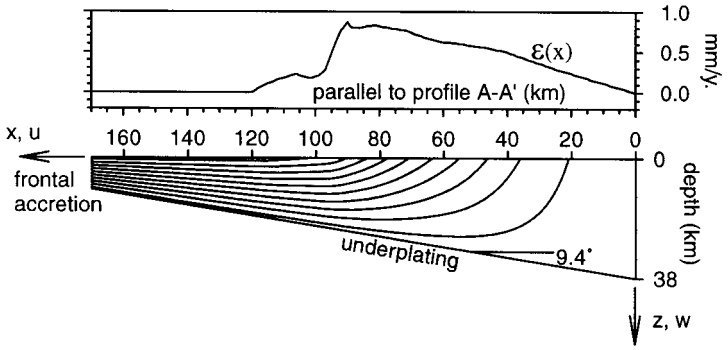

Fig. A1. Layout for the kinematic model, with x indicating distance along A-A′ from an origin located at the back of the wedge (northeast coast of the Olympic Peninsula) and z indicating depth. The west coast lies at $x = 120$ km, and the shelf edge at $x = 170$ km. The position of the base of the wedge is based on the distribution of Benioff zone seismicity, which is inferred to occur mainly in the uppermost mantle of the Juan de Fuca plate (Brandon and Calderwood, 1990). The model calculation produces velocity fields that are consistent with observed erosion rates ε(x) at the surface of the wedge (upper plot), as given in figure 19. Horizontal and vertical velocities, u and w respectively, are relative to a fixed point at the origin.

wedge. Following Brandon, Roden-Tice, and Garver (1998) and the results summarized here, we assume that the velocity field has been two dimensional (that is, plane strain) and steady over a time scale of at least several million years. The rocks that make up the wedge are assumed to have negligible compressibility. Thus, the continuity equation requires that $\frac{\partial u}{\partial x} = -\frac{\partial w}{\partial z}$, where position is described by x and z, and velocity is defined by

$$u = \frac{dx}{dt} \text{ and } w = \frac{dz}{dt}.$$

Velocities are specified relative to the back of the wedge, which is defined by the eastern limit of the Olympic Mountains, where topography drops to sealevel at the west side of Puget Sound. Velocities are set to zero there, as indicated by $u(0, z) = w(0, z) = 0$. Vertical velocities at the surface of the wedge are defined by

$$w(x, 0) = -\epsilon(x), \tag{A-1}$$

where $\epsilon(x)$ is the long-term erosional flux through the top of the wedge section. For our calculations, we use the best-fit estimate of $\epsilon(x)$ shown in figure 19. For accretionary fluxes into the wedge, we use two end-member cases to defined a continuum of possibilities: (1) frontal accretion where the influx of material occurs entirely through the front of the wedge, and (2) underplating accretion, where the influx is limited to the base of the wedge. The specifics of these two accretionary options are given below but note that the steady-state condition specifies that the accretionary influx is equal to the erosional outflux. We assume that there is no flux through the back of the wedge, which is consistent with evidence that the east side of the Olympics uplift has not advanced eastward relative to Puget Sound. The onset of accretion into the back side of the wedge would be indicated by east-vergent imbricate faulting within a low-taper wedge front (Willett, Beaumont, and Fullsack, 1993).

We consider the velocity field within a domain that extends from the east side of the Olympics uplift at $x = 0$ to the shelf edge at $x = 170$ km and extends from the surface of the wedge to the subducting Juan de Fuca slab. Following Brandon and Calderwood (1990), we define the top of the slab by $h(x) = h_0 - x \tan \theta$, with $h_o = 38$ km and $\theta = 9.4°$ (fig. A-1).

We make a simplying assumption that the vertical gradient in the horizontal component of the velocity field can be ignored for our problem, so that $\frac{\partial u}{\partial z} = 0$. This approach, which has been used in other types of kinematic modeling (Holt and Haines, 1995), is reasonable because we are mainly interested in exploring the general relationship at the surface of the wedge between the vertical velocity component as recorded by strath uplift and erosional fluxes, and the horizontal velocity component as recorded by the offset sea cliff

and by geodetic measurements. The physical sense of this assumption is that beneath every point at the surface, horizontal velocities are represented by a single vertical-averaged value, so that $u(x,z) = u(x,0)$.

For frontal accretion alone, the erosional flux out of the top of the wedge between the origin and x must be balanced by an accretionary flux into the wedge crossing the vertical boundary beneath x, which is specified by $\int_0^x \epsilon(x)\,dx = -h(x)\,u(x,0)$. This relationship can be recast to give,

$$u(x,z)_F = \frac{-1}{h(x)} \int_0^x \epsilon(x)\,dx, \tag{A-2}$$

where the subscript F indicates that the horizontal velocity is for frontal accretion alone. The continuity equation indicates that

$$\int_{w(x,0)}^{w(x,z)} dw = -\int_0^z \frac{\partial u}{\partial x}\,dz.$$

Substitution of A-1 and A-2 gives the vertical velocity for frontal accretion alone,

$$w(x,z)_F = \left[1 + \frac{z}{h(x)}\right]\epsilon(x) + \frac{z \tan\theta}{h^2(x)} \int_0^x \epsilon(x)\,dx. \tag{A-3}$$

The end-member case for accretion by underplating is represented here by

$$u(x,z)_B = 0, \tag{A-4}$$

and

$$w(x,z)_B = \epsilon(x). \tag{A-5}$$

The subscript B indicates that these velocities are due to underplating alone. The underlying assumption for these equations is that the erosion-rate profile mimics the underlying pattern of underplating; motion only occurs in the vertical direction, resulting in a vertically-shearing velocity field.

Cases intermediate between underplating and frontal accretion can be specified by a combination of the two end-member velocity fields,

$$u(x,z) = \alpha\, u(x,z)_F + (1-\alpha)u(x,z)_B, \tag{A-6}$$

and

$$w(x,z) = \alpha\, w(x,z)_F + (1-\alpha)w(x,z)_B, \tag{A-7}$$

where α indicates the proportion of frontal accretion relative to total accretion.

The velocity field given by A-6 and A-7 can be used to calculate the horizontal strain rate $D_{xx} = \frac{\partial u}{\partial x}$, which is used in the text to compare model results to short-term horizontal strain rates measured by Savage, Lisowski, and Prescott (1991). The two end-member velocity fields used here were selected, in part, to represent a maximum range of horizontal velocities and horizontal strain rates. The horizontal velocities and strain rates for the underplating velocity field (A-4, -5) are everywhere zero, whereas the frontal accretion velocity field (A-2, -3) has the largest possible horizontal velocities and shortening rates.

REFERENCES

Adams, J., 1984, Active deformation of the Pacific Northwest continental margin: Tectonics, v. 3, p. 449–472.

Anderson, R. S., Densmore, A. L., and Ellis, M. A., 1999, The generation and degradation of marine terraces: Drainage Research, v. 11, p. 7–19.

Armentrout, J. M., 1981, Correlation and ages of Cenozoic chronostratigraphic units in Oregon and Washington, *in* Armentrout, J. M., editor, Pacific Northwest Cenozoic biostratigraphy: Geological Society of America Special Paper 184, p. 137–148.

Atwater, B. F., 1987, Evidence for great Holocene earthquakes along the outer coast of Washington State: Science, v. 236, p. 942–944.

——— 1996, Coastal evidence for great earthquakes in western Washington, *in* Rogers, A. M., Walsh, T. J., Kockelman, W. J., and Priest, G. R., editors, Assessing earthquake hazards and reducing risk in the Pacific Northwest; Volume 1.: United States Geological Survey Professional Paper 1560, p. 77–90.

Batt, G. E., Brandon, M. T., Farley, K. A., and Roden-Tice, M., in press, Tectonic synthesis of the Olympic Mountains segment of the Cascadia wedge, using 2-D thermal and kinematic modeling of isotopic ages: Journal of Geophysical Research.

Beaumont, C., Ellis, S., and Pfiffner, A., 1999, Dynamics of subduction-accretion at convergent margins: Short-term modes, long-term deformation, and tectonic implications: Journal of Geophysical Research, v. 104, p. 17,573–17,602.

Bigelow, P. K., ms, 1987, The petrology, stratigraphy and drainage history of the Montesano Formation, southwestern Washington and Southern Olympic Peninsula: M.S. thesis, Western Washington University, Bellingham, Washington, 263 p.

Bockheim, J., G., Kelsey, H. M., and Marshall, J. G., III., 1992, Soil development, relative dating, and correlation of late Quaternary marine terraces in southwestern Oregon: Quaternary Research, v. 37, p. 60–74.

Brandon, M. T., 1996, Probability density plots for fission-track grain age distributions: Radiation Measurements, v. 26, p. 663–676.

Brandon, M. T., and Calderwood, A. R., 1990, High-pressure metamorphism and uplift of the Olympic subduction complex: Geology, v. 18, p. 1252–1255.

Brandon, M. T., Roden-Tice, M. K., and Garver, J. I., 1998, Late Cenozoic exhumation of the Cascadia accretionary wedge in the Olympic Mountains, northwest Washington State: Geological Society of America Bulletin, v. 110, p. 985–1009.

Brandon, M. T., and Vance, J. A., 1992, Tectonic evolution of the Cenozoic Olympic subduction complex, Washington State, as deduced from fission track ages for detrital zircons: American Journal of Science, v. 292, p. 565–636.

Bucknam, R. C., Hemphill-Haley, E., and Leopold, E. B., 1992, Abrupt uplift within the past 1700 years at southern Puget Sound, Washington: Science, v. 258, p. 1611–1614.

Bull, W. B., 1991, Geomorphic response to climatic change: New York, Oxford University Press, 326 p.

Burbank, D. W., Leland, J., Fielding, E., Anderson, R. S., Brozovic, N., Reid, M. R., and Duncan, C., 1996, Bedrock incision, rock uplift and threshold hillslopes in the northwestern Himalayas: Nature, v. 379, p. 505–510.

Byrne, D., Wang, W., and Davis, D., 1993, Mechanical role of backstops in the growth of forearcs: Tectonics, v. 12, no. 1, p. 123–144.

Campbell, K. A. and Nesbitt, E. A., 2000, High resolution architecture and paleoecology of an active margin, storm-flood influenced estuary, Quinault Formation (Pliocene), Washington: Palaios, v. 15, n. 6, p. 553–579.

Chappell, J., Omura, A., Esat, T., McCulloch, M., Pandolfi, J., Ota, Y., and Pillans, B., 1996, Reconciliation of late Quaternary sealevels derived from coral terraces at Huon Peninsula with deep sea oxygen isotope records: Earth and Planetary Science Letters, v. 141, p. 227–236.

Chinn, T., 1981, Use of rock weathering-rind thickness for Holocene absolute age-dating in New Zealand: Arctic and Alpine Research, v. 13, p. 33–45.

Cleveland, W. S., 1979, Robust locally weighted regression and smoothing scatterplots: Journal of the American Statistics Association, v. 74, p. 829–836.

——— 1981, LOWESS: A program for smoothing scatterplots by robust locally weighted regression: American Statistician, v. 35, p. 54.

Clowes, R. M., Brandon, M. T., Green, A. C., Yorath, C. J., Sutherland Brown, A., Kanasewich, E. R., and Spencer, C., 1987, LITHOPROBE - southern Vancouver Island: Cenozoic subduction complex imaged by deep seismic reflections: Canadian Journal of Earth Sciences, v. 24, p. 31–51.

Colman, S. M. and Pierce, K., 1981, Weathering rinds on andesitic and basaltic stones as a Quaternary age indicator, western United States: United States Geological Survey Professional Paper 1210, 56 p.

——— 1986, Glacial sequence near McCall, Idaho; weathering rinds, soil development, morphology, and other relative-age criteria: Quaternary Research, v. 25, p. 25–42.

Crandell, D. R., 1964, Pleistocene glaciations of the southwestern Olympic Peninsula, Washington: United States Geological Survey Professional Paper 501-B, p. B135–B139.

——— 1965, The glacial history of western Washington and Oregon, *in* Wright, H.E., and Frey, D.G., editors, The Quaternary of the United States: Princeton, New Jersey, Princeton University Press, p. 341–353.

Crosson, R. S., and Owens, T. J., 1987, Slab geometry of the Cascadia subduction zone beneath Washington from earthquake hypocenters and teleseismic converted waves: Geophysical Research Letters, v. 14, p. 824–827.

Darienzo, M. E. and Peterson, C. D., 1990, Episodic tectonic subsidence of late Holocene salt marshes, northern Oregon coast, central Cascadia margin, U.S.A.: Tectonics, v. 9, p. 1–22.

Daly, C., and Taylor, G., 1998, Washington Average Monthly or Annual Precipitation, 1961-90, Available: *http://www.ocs.orst.edu/prism/prism_new.html*; also published by: Water and Climate Center of the Natural Resources Conservation Service, Portland, Oregon.

Dean, R., 1991, Equilibrium beach profiles: Characteristics and Applications: Journal of Coastal Research, v. 7, no. 1, p. 53–84.

DeMets, C., and Dixon, T., 1999, New kinematic models for Pacific-North America motion from 3 Ma to present; I, Evidence for steady motion and biases in the NUVEL-1A model: Geophysical Research Letters, v. 26, no. 13, p. 1921–1924.

DeMets, C., Gordon, R. G., Argus, D. F., and Stein, S., 1990, Current plate motions: Geophysical Journal International, v. 101, p. 425–478.

Dragert, H., 1987, The fall (and rise) of central Vancouver Island: 1930-1985: Geological Survey of Canada Contribution 10586, p.689–697.

Dragert, H., Hyndman, R. D., Rogers, G. C., and Wang, K., 1994, Current deformation and the width of the seismogenic zone of the northern Cascadia subduction thrust: Journal of Geophysical Research B, v. 99, p. 653–668.
Easterbrook, D. J., 1986, Stratigraphy and chronology of Quaternary deposits of the Puget lowland and Olympic Mountains of Washington and the Cascade Mountains of Washington and Oregon, *in* Sibrava, V., Bowen, D.Q., and Richmond, G.M., editors, Quaternary glaciations in the northern hemisphere: Quaternary Science Reviews, v. 5, p. 145–159.
Florer, L. E., 1972, Quaternary paleoecology and stratigraphy of the sea cliffs, western Olympic Peninsula, Washington: Quaternary Research, v. 2, p. 202–216.
Fuller, I. C., Macklin, M. G., Lewin, J., Passmore, D. G., and Wintle, A. G., 1998, River response to high-frequency climate oscillations in southern Europe over the past 200 k.y.: Geology, v. 26, p. 275–278.
Heusser, C. J., 1964, Palynology of four bog sections from the western Olympic Peninsula, Washington: Ecology, v. 45, p. 23–40.
——— 1972, Palynology and phytogeographical significance of a late Pleistocene refugium near Kalaloch, Washington: Quaternary Research, v. 2, p. 189–201.
——— 1973, Environmental sequence following the Fraser advance of the Juan de Fuca lobe, Washington: Quaternary Research, v. 3, p. 284–306.
——— 1974, Quaternary vegetation, climate, and glaciation of the Hoh River Valley, Washington: Geological Society of American Bulletin, v. 85, p. 1547–1560.
——— 1978, Palynology of Quaternary deposits of the lower Bogachiel River area, Olympic Peninsula, Washington: Canadian Journal of Earth Sciences, v. 15, p. 1568–1578.
Holdahl, S. R., Faucher, F., and Dragert, H., 1989, Contemporary vertical crustal motion in the Pacific northwest, *in* Cohen, S. C. and Vanicek, P., editors, Slow deformation and transmission of stress in the earth: American Geophysical Union, Geophysical Monograph 40, International Union of Geodesy and Geophysics Volume 4, p. 17–29.
Holt, W. E., and Haines, A. J., 1995, The kinematics of northern South Island, New Zealand, determined from geologic strain rates: Journal of Geophysical Research, v.100, p. 17991–18010.
Hovius, N., 2000, Macro-scale process systems of mountain belt erosion, *in* Summerfield, M. A., editor, Geomorphology and Global Tectonics: London, John Wiley and Sons, p. 77–105.
Hyndman, R. D., and Wang, K., 1993, Thermal constraints on the zone of major thrust earthquake failure: the Cascadia subduction zone: Journal of Geophysical Research, v. 98, p. 2039–2060.
James, T. D., Clague, J. J., Wang, K., and Hutchinson, I., 2000, Post-glacial rebound at the northern Cascadia subduction zone: Quaternary Science Reviews, v. 19, p. 1527–1541.
Kelsey, H. M., 1990, Late Quaternary deformation of marine terraces on the Cascadia subduction zone near Cape Blanco, Oregon: Tectonics, v.9, p. 983–1014.
Kelsey, H. M. and Bockheim, J. G., 1994, Coastal landscape evolution as a function of eustasy and surface uplift rate, Cascadia margin, southern Oregon: Geological Society of America Bulletin, v. 106, p. 840–854.
Knox, J. C., 1975, Concept of the graded stream, *in* Melhorn, W. N. and Flemal, R. C., editors, Theories of Landform Development, Proceedings of the 6th Geomorphology Symposium, Publications in Geomorphology: Binghamton, State University of New York at Binghamton, p. 169–198.
Knuepfer, P. L. K., 1988, Estimating ages of late Quaternary stream terraces from analysis of weathering rinds and soils: Geological Society of America Bulletin, v. 100, p. 1224–1236.
Koons, P., 1990, Two-sided orogen; collision and erosion from the sandbox to the Southern Alps, New Zealand: Geology, v. 18, p. 679–682.
Lajoie, K. R., 1986, Coastal tectonics, *in* Wallace, R. E. editor, Active Tectonics: Washington, D.C., National Academy of Sciences, p. 95–124.
Leopold, L. B. and Bull, W. B., 1979, Base level, aggradation, and grade: Proceedings of the American Philosophical Society, v. 123, p. 168–202.
McCrory, P. A., 1996, Tectonic model explaining divergent contraction directions along the Cascadia subduction margin, Washington: Geology, v. 24, p. 929–932.
——— 1997, Evidence for Quaternary tectonism along the Washington Coast: Washington Geology, v. 25, p. 14–19.
McNeill, L., Piper, K., Goldfinger, C., Kulm, L., and Yeats, R., 1997, Listric normal faulting on the Cascadia continental margin: Journal of Geophysical Research B, v. 102, p. 12,123–12,138.
McNeill, L. C., Goldfinger, C., Kulm, L. D., Yeats, R. S., 2000, Tectonics of the Neogene Cascadia forearc drainage; investigations of a deformed late Miocene unconformity: Geological Society of America Bulletin, v. 112, p. 1209–1224.
Mackin, J. H., 1948, Concept of the graded river: Geological Society of America Bulletin, v. 59, p. 463–512.
McSaveney, M., 1992, A manual of weathering-rind dating for sandstone clasts of the Torlesse Supergroup: Geological Society of New Zealand Miscellaneous Publication 63A, 106 p.
Maddy, D., 1997, Uplift-driven valley incision and river terrace formation in southern England: Journal of Quaternary Science, v. 12, p. 539–545.
Mitchell, C. E., Vincent, P., Weldon R. J., and Richards, M., 1994, Present-day vertical deformation of the Cascadia margin, Pacific Northwest, U.S.A.: Journal of Geophysical Research B, v. 99, p. 12,257–12,277.
Moore, J. L., ms, 1965, Surficial geology of southwestern Olympic Peninsula: M.S. thesis, University of Washington, Seattle, Washington, 63 p.
Muhs, D. R., 1992, The last interglacial-glacial transition in North America: Evidence from uranium-series dating of coastal deposits, *in* Clark, K. P., and Lea, P. D., editors, The Last Interglacial-Glacial Transition in North America, Geological Society of America Special Paper, p. 31–51.

National Data Buoy Center, 2000, Station Information, U.S. Northwest Region. *http://seaboard.ndbc.noaa.gov/stuff/northwest/nwstmap.shtml*

Orange, D. L., 1990, Criteria helpful in recognizing shear-zone and diapiric melanges: Examples from the Hoh accretionary complex, Olympic Peninsula, Washington: Geological Society of America Bulletin, v. 102, p. 935–951.

Ouchi, S., 1985, Response of alluvial rivers to slow active tectonic movements: Geological Society of America Bulletin, v. 96, p. 504–515.

Palmer, S. P., and Lingley, W. S., Jr., 1989, An assessment of the oil and gas potential of the Washington outer continental shelf: University of Washington, Washington Sea Grant Program, p. 83.

Parsons, T., Trehu, A. M., Luetgert, J. H., Miller, K. C., Kilbride, F., Wells, R. E., Fisher, M. A., Flueh, E. R., ten Brink, U. S., Christensen, N. I., 1998, A new view into the Cascadia subduction zone and volcanic arc; implications for earthquake hazards along the Washington margin: Geology, v. 26, no. 3, p. 199–202.

Pazzaglia, F. J., Gardner, T. W., and Merritts, D., 1998, Bedrock fluvial incision and longitudinal profile development over geologic time scales determined by fluvial terraces, *in* Wohl E. and Tinkler, K., editors, Rivers over rock, Fluvial Processes in Bedrock Channels: American Geophysical Union, Geophysical Monograph Series, 107, p. 207–236.

Personius, S. F., 1995, Late Quaternary stream incision and uplift in the forearc of the Cascadia subduction zone, western Oregon: Journal of Geophysical Research B, v. 100, p. 20,193–20,210.

Pillans, B., Chappell, J., and Naish, T. R., 1998, A review of the Milankovitch climatic beat: template for Plio-Pleistocene sea-level changes and sequence stratigraphy: Sedimentary Geology, v. 122, p. 5–21.

Porter, S. C., Pierce, K. L., and Hamilton, T. D., 1983, Late Wisconsin mountainous glaciation in the Western United States, *in* Wright, H. E., editor, Late Quaternary Environments of the United States, Volume 1, The Late Pleistocene: Minneapolis, University of Minnesota Press, p. 71–114.

Posamentier, H. W., Jervey, M. T., and Vail, P. R., 1988, Eustatic controls on clastic deposition; I, Conceptual framework, in Wilgus Cheryl, K., Hastings Bruce, S., Ross Charles, A., Posamentier Henry, W., Van Wagoner, J., and Kendall Christopher, G. S. C., editors, Sea-level changes; an integrated approach.: Special Publication - Society of Economic Paleontologists and Mineralogists: Tulsa, Oklahoma, United States, SEPM (Society for Sedimentary Geology), p. 109–124.

Rau, W. W., 1970, Foraminifera, stratigraphy, and paleoecology of the Quinault Formation, Point Grenville-Raft River coastal area, Washington: Washington Department of Natural Resources Bulletin, v. 62, 34 p.

——— 1973, Geology of the Washington coast between Point Grenville and the Hoh River: Washington Department of Natural Resources, Geology and Earth Resources Division Bulletin 66, 58 p.

——— 1975, Geologic map of the Destruction Island and Taholah quadrangles, Washington: Washington Department of Natural Resources, Geology and Earth Resources Division Map GM-13, scale 1:62,500.

——— 1979, Geologic map in the vicinity of the lower Bogachiel and Hoh River valleys and the Washington coast: Department of Natural Resources, Geology and Earth Resources Division Map GM-24, scale 1:62,500.

Rau, W. W., and Grocock, G., 1974, Piercement structure outcrops along the Washington coast: State of Washington, Department of Natural Resources, Division of Mines and Geology, Information Circular, v. 51, 7 p.

Reilinger, R. and Adams, J., 1982, Geodetic evidence for active landward tilting of the Oregon and Washington Coastal ranges: Geophysical Research Letters, v. 9, p. 401–403.

Ricker, K., Chinn, T., and McSaveney, M., 1993, A late Quaternary moraine sequence dated by rock weathering rinds, Craigieburn Range, New Zealand: Canadian Journal of Earth Sciences, v. 30, p. 1861–1869.

Rogers, G. C., 1988, An assessment of megathrust earthquake potential of the Cascadia subduction zone: Canadian Journal of Earth Science, v. 25, p. 844–852.

Saunders, I.R., Clague, J.J., and Roberts, M.C., 1987, Deglaciation of the Chilliwack River valley, British Columbia: Canadian Journal of Earth Science, v. 24, p. 915–923.

Savage, J. C., Lisowski, M., and Prescott, W. H., 1981, Geodetic strain measurements in Washington: Journal of Geophysical Research B, v. 86, p. 4929–4940.

——— 1991, Strain accumulation in western Washington: Journal of Geophysical Research B, v. 96, p. 14,493–14,507.

Schumm, S. A., 1969, River metamorphosis: Proceedings of the American Society of Civil Engineers, Journal of the Hydraulics Division, v. 95, p. 255–273.

——— 1973, Geomorphic thresholds and complex response of drainage systems, *in* Morisawa, M., editor, Fluvial Geomorphology: Proceedings of the 4th Geomorphology Symposium, Publications in Geomorphology: Binghamton, State University of New York at Binghamton, p. 299–310.

Schumm, S. A., Dumont, J. F., and Holbrook, J. M., 2000, Active tectonics and alluvial rivers: Cambridge, United Kingdom, Cambridge University Press, 276 p.

Schumm, S. A. and Lichty, R. W., 1965, Time, space, and causality in geomorphology: American Journal of Science, v. 263, p. 110–119.

Soil Survey Staff, 1975, Soil Taxonomy: A basic system of soil classification for making and interpreting soil surveys: United States Department of Agriculture Handbook 436, 754 p.

Tabor, R. W. and Cady, W. M., 1978a, Geologic Map of the Olympic Peninsula: United States Geological Survey Map I-994, 2 sheets, scale 1:125,000.

——— 1978b, The structure of the Olympic Mountains, Washington - analysis of a subduction zone: United States Geological Survey Professional Paper 1033, 38 p.

Thackray, G. D., ms, 1996, Glaciation and neotectonic deformation on the western Olympic Peninsula, Washington: Ph.D. dissertation, University of Washington, Seattle, Washington, 139 p.

——— 1998, Convergent-margin deformation of Pleistocene strata on the Olympic coast of Washington, USA, *in* Stewart, I. S. and Vita-Finzi, C., editors, Coastal Tectonics: London, Geological Society Special Publication 146, p. 199–211.

——— 2001, Extensive Early and Middle Wisconsin glaciation on the western Olympic Peninsula, Washington, and the variability of Pacific moisture delivery to the northwestern United States: Quaternary Research, v. 55, p. 257–270.

Thackray, G. D. and Pazzaglia, F. J., 1994, Quaternary stratigraphy, tectonic geomorphology, and fluvial evolution of the western Olympic Peninsula, Washington, *in* Swanson, D.A., and Haugerud, R.A., editors, Geologic field trips in the Pacific Northwest, 1994 Geological Society of America Annual Meeting, Seattle, Washington, p. 2A-1 - 2A-30.

Thorson, R. M., 1989, Glacio-isostatic response of the Puget Sound area, Washington: Geological Society of America Bulletin, v. 101, p. 1163–1174.

Trenhaile, A., 1997, Coastal Dynamics and Landforms: Oxford, Clarendon Press, 366 p.

von Huene, R., 1998, Forearc highs and backstop structure, Eos, Transactions, American Geophysical Union, v. 79, p. F917.

von Huene, R., D. Klaeschen, M. Gutscher, and J. Fruehn, 1998, Mass and fluid flux during accretion at the Alaskan margin: Geological Society of America Bulletin, v. 110, p. 468–482.

Washington State Department of Transportation, 1988, Queets River Bridge Replacement: Geotechnical Report SR101, L-8287, C.S. 1601, No. 101/204 Replacement.

Wegmann, K., ms, 1999, Tectonic geomorphology of the Clearwater River drainage, Olympic Peninsula, Washington: M.S. thesis, Albuquerque, University of New Mexico, 217 p.

Weldon, R. J., ms, 1986, Late Cenozoic geology of Cajon Pass; implications for tectonics and sedimentation along the San Andreas fault:Ph.D. dissertation, California Institute of Technology, Pasadena, California, 400 p.

West, D. O., and McCrumb, D. R., 1988, Coastline uplift in Oregon and Washington and the nature of Cascadia subduction zone tectonics: Geology, v. 16, p. 169–172.

Willett, S., 1999, Orogeny and orography: The effects of erosion on the structure of mountain belts: Journal of Geophysical Research v. 104, p. 28,957–28,981.

Willett, S., Beaumont, C., and Fullsack, P., 1993, Mechanical models for the tectonics of doubly vergent compressional orogens: Geology, v. 21, p. 371–374.

Willett, S. D., Slingerland, R., and Hovius, N., 2001, Uplift, shortening, and steady state topography in active mountain belts: American Journal of Science, v. 301, p.

Yeats, R. S., Graven, E. P., Werner, K. S., Goldfinger, C., and Popowski, T. A., 1996, Tectonics of the Willamette Valley, Oregon, *in* Rogers, A. M., Walsh, T. J., Kockelman, W. J., and Priest, G. R., editors, Assessing earthquake hazards and reducing risk in the Pacific Northwest; Volume 1.: United States Geological Survey Professional Paper 1560, p.